Atmos. Chem. Phys., 9, 685–706, 2009
www.atmos-chem-phys.net/9/685/2009/

Atmospheric Chemistry and Physics

Modelling of cirrus clouds – Part 1a: Model description and validation

P. Spichtinger[1] **and K. M. Gierens**[2]

[1]Institute for Atmospheric and Climate Science, ETH Zurich, 8092 Zurich, Switzerland
[2]Deutsches Zentrum für Luft- und Raumfahrt, Institut für Physik der Atmosphäre, Oberpfaffenhofen, Germany

Received: 16 November 2007 – Published in Atmos. Chem. Phys. Discuss.: 11 January 2008
Revised: 23 October 2008 – Accepted: 1 December 2008 – Published: 28 January 2009

Abstract. A double-moment bulk microphysics scheme for modelling cirrus clouds including explicit impact of aerosols on different types of nucleation mechanism is described. Process rates are formulated in terms of generalised moments of the underlying a priori size distributions in order to allow simple switching between various distribution types. The scheme has been implemented into a simple box model and into the anelastic non-hydrostatic model EULAG. The new microphysics is validated against simulations with detailed microphysics for idealised process studies and for a well documented case of arctic cirrostratus. Additionally, the formation of ice crystals with realistic background aerosol concentration is modelled and the effect of ambient pressure on homogeneous nucleation is investigated in the box model.

The model stands all tests and is thus suitable for cloud-resolving simulations of cirrus clouds.

1 Introduction

The role of clouds is crucial for our understanding of the current and the changing climate (IPCC, 2007). Cirrus clouds modulate the Earth's radiation budget significantly. It is assumed that (thin) cirrus clouds contribute to a net warming of the Earth-Atmosphere system (e.g. Chen et al., 2000), but the magnitude of this warming has not been quantified yet. Recently, the impact of thin cirrus clouds in the mid latitudes was estimated in idealised framework using vertical profiles from radiosondes (Fusina et al., 2007), but the global effect is still uncertain. The formation and evolution of cirrus clouds depends in a complex way on a variety of environmental conditions (temperature, relative humidity, wind fields) as well as on the impact of background aerosol acting as ice nuclei. The interaction of various processes and their non-linear dependence on ambient conditions renders the understanding of cirrus clouds in general a difficult task.

Cirrus clouds (except anvils) are closely related to their formation regions, so-called ice-supersaturated regions (ISSRs, see e.g. Gierens et al., 1999). These are large, initially cloud free airmasses in the upper troposphere (and sometimes lowermost stratosphere) in the status of supersaturation with respect to (wrt) ice. These regions are quite frequent in the tropopause region (see e.g. Spichtinger et al., 2003a,b; Gettelman et al., 2006). From former investigations (Spichtinger et al., 2005a) it turns out that cirrus clouds often are embedded in horizontally extended ISSRs; ISSRs and their embedded clouds form a system. Large-scale dynamical processes like synoptic upward motions, but also mesoscale waves and small scale turbulence play crucial roles for the formation and evolution of the system ISSR/cirrus (Spichtinger et al., 2005a,b). Local dynamics and microphysics are acting on the cloud and sub cloud-scale. From this point of view there is need of a cloud resolving model which can be used for idealised studies of cirrus clouds interacting with various scales of dynamics.

While from theory and measurements it is quite understood that in cloud free air masses the relative humidity wrt ice can reach very high values up to the freezing thresholds for homogeneous freezing (i.e. 140–170% RHi, depending on temperature, see Koop et al., 2000), substantial and persistent supersaturation inside cirrus clouds is more difficult to understand. Ice crystals act as a strong sink for water vapour. Thus, one expects that RHi-distributions inside cirrus are centred around saturation, as some measurements indicate (Ovarlez et al., 2002; Spichtinger et al., 2004). However, there are also many measurements from inside cirrus clouds that indicate considerable degrees of supersaturation (see Comstock et al., 2004; Lee et al., 2004; Ovarlez et al., 2002; Krämer et al., 2008; Peter et al., 2008, and M. Krämer, personal communication). These findings seem to

Correspondence to: P. Spichtinger
(peter.spichtinger@env.ethz.ch)

be contrary to our current understanding of microphysics inside cirrus clouds (Peter et al., 2006) and call for an explanation. One possible explanation will be given in the present paper. Another pending question is the impact of different nucleation mechanisms on the formation and evolution of cirrus clouds. While it is generally assumed that homogeneous nucleation is the dominant formation process for cold ($T<-38°$C) cirrus clouds (e.g. Sassen and Dodd, 1988; Heymsfield and Sabin, 1989; Haag et al., 2003b), there are indications that heterogeneous nucleation can substantially modify the conditions for homogeneous nucleation bringing forth large change in resulting cloud properties. Therefore a model for studying the competition of different nucleation processes would be useful.

Cirrus clouds have been modelled on all scales: there are large scale models for climate research and numerical weather prediction (Kärcher et al., 2006; Liu et al., 2007; Tompkins et al., 2007) and mesoscale models (Harrington et al, 1995; Reisner et al., 1998; Phillips et al., 2003; Seifert and Beheng, 2005). For detailed process studies, cloud resolving models (Starr and Cox, 1985; Jensen et al., 1994; Lin et al., 2005; Kärcher, 2005) and box models (Sassen and Dodd, 1989; Lin et al., 2002; Gierens, 2003; Haag and Kärcher, 2004; Hoyle et al., 2005; Bunz et al., 2008) were used. Many box models and cloud resolving models have very detailed microphysics schemes which require high spatial and temporal resolution. Large scale and mesoscale models often use bulk microphysics schemes.

We have developed a new ice microphysics scheme for the use in box models and cloud resolving models, based on earlier work (Gierens, 2003). A novel feature of the model is the use of arbitrary many classes of ice, discriminated by their formation mechanism. The corresponding aerosol types that are involved in the formation of the various ice classes are treated as well. This new concept allows us to investigate the impact of different nucleation processes in the same airmass, in particular how air pollution (heterogeneous nucleation) affects the cloud evolution. Another novel feature is the formulation of the various process rates in terms of moments of the underlying crystal size distribution. This makes it possible to the choose between various distribution types.

The structure of this article is as follows: in the next section we will describe the basic dynamical models, i.e. the box model and the anelastic, non-hydrostatic model EULAG very briefly. In Sect. 3 the new microphysics scheme is described in detail. In Sect. 4 the validation of the model using box model simulations and 1-D simulations is shown, and the model's performance is discussed. We end with a summary and draw conclusions in Sect. 5.

2 Model description – dynamics

The new microphysics scheme is implemented into two different types of models: First, we implemented the ice microphysics into a simple box model for validating the nucleation parameterisation and for fast calculations serving a principal understanding of the interaction of different processes. The box model can also be coupled to trajectories, e.g. to the output of a trajectory model (in our case LAGRANTO, Wernli and Davies, 1997). In a second step we implemented the tested microphysics into the anelastic, non-hydrostatic model EULAG (Smolarkiewicz and Margolin, 1997). The twofold approach was not only for testing the model but also to have two different tools which can be used for different applications, which have exactly the same ice microphysics parameterisations.

In the following we describe first the more complex dynamics of the EULAG model and the coupling of the dynamics to the microphysics.

Then, we describe the box model which was developed together with the microphysics in the spirit of the EULAG model, i.e. using background states (e.g. for potential temperature) as well. This choice was made to make the "transition" between the two models as smooth as possible.

2.1 EULAG model – dynamics

As a basic dynamical model we use the anelastic nonhydrostatic model EULAG (see e.g. Smolarkiewicz and Margolin, 1997). The anelastic equations for the dry dynamics can be written in perturbation form as follows (cf. Smolarkiewicz et al., 2001; Grabowski and Smolarkiewicz, 2002)

$$\frac{D\mathbf{u}}{Dt} = -\nabla\left(\frac{p'}{\bar{\rho}}\right) + \mathbf{g}\left(\frac{\theta'}{\bar{\theta}}\right) - \mathbf{f}\times\mathbf{u}' + \mathbf{M} \tag{1}$$

$$\frac{D\theta'}{Dt} = -\mathbf{u}\cdot\nabla\theta_e \tag{2}$$

Here, $\mathbf{u}$ is the velocity vector; p, ρ and θ denote pressure, density and potential temperature, respectively; $\mathbf{g}$ and $\mathbf{f}$ denote gravity and "Coriolis" vectors, respectively; $\bar{\theta}$ and $\bar{\rho}$ are the anelastic reference state profiles for potential temperature and density; $\mathbf{M}$ denotes additional appropriate metric terms, depending on the coordinate system chosen. The subscript e refers to the environmental profiles, which must not necessarily be equal to the reference states. Primes denote deviations from the environmental state (e.g. $\theta'=\theta-\theta_e$). $\frac{D}{Dt} := \partial/\partial t + \mathbf{u}\cdot\nabla$ denotes the total derivative. The perturbation pressure p' is calculated using the mass continuity constraint $\nabla\cdot\bar{\rho}\mathbf{u}=0$.

For solving the governing equations we use the unified semi-Lagrangian-Eulerian approach described in Smolarkiewicz and Margolin (1997); Smolarkiewicz et al. (2001): Let Ψ and $\mathbf{F}$ denote the vectors of variables (θ', u, v, w) and their forcings, respectively. With $\tilde{\Psi} := \Psi^n + 0.5\Delta t\mathbf{F}^n$ and the generalised transport operator LE the approximation can be described as

$$\Psi_{\mathbf{i}}^{n+1} = LE_{\mathbf{i}}\left(\tilde{\Psi}\right) + 0.5\Delta t\mathbf{F}_{\mathbf{i}}^{n+1} \tag{3}$$

whereby **i** and n denote the spatial and temporal location, respectively. This results into a trapezoidal rule for the approximations. This treatment and the non-oscillatory forward-in-time (NFT) semi-Lagrangian/Eulerian approximations of the integrals were carried out as described in detail in Smolarkiewicz and Margolin (1997) and Smolarkiewicz et al. (2001). The model was used for many applications on different scales and several problems in atmospheric dynamics (e.g. stratified flow over mountains, convectively induced gravity waves etc.). One main advantage of this model is the less diffusive advection scheme MPDATA (Multidimensional Positive Definite Advection Transport Algorithm, see e.g. Smolarkiewicz and Margolin, 1998).

For including cloud physics into the model, we have to perform "moist" dynamics and a coupling of dynamics and thermodynamics. This can be done as follows (see also Grabowski and Smolarkiewicz, 2002): We define the density potential temperature (see Emanuel, 1994) including specific humidity q_v and the mixing ratio of cloud ice q_c as follows:

$$\theta_d := \theta + \bar{\theta}(\epsilon_p\, q_v - q_c) \tag{4}$$

with $\epsilon_p = (1/\epsilon) - 1$, where $\epsilon = R_g/R_v$ denotes the ratio of the ideal gas constants for dry air and water vapour, respectively. Using the definition of an environmental density potential temperature $\theta_{de} := \theta_e + \bar{\theta}\,\epsilon_p\, q_{ve}$ for the representation of the perturbation $\theta'_d = \theta_d - \theta_{de}$ the governing equations for the moist dynamics read as follows:

$$\frac{D\mathbf{u}}{Dt} = -\nabla\left(\frac{p'}{\bar{\rho}}\right) + \mathbf{g}\left(\frac{\theta'_d}{\bar{\theta}}\right) - \mathbf{f}\times\mathbf{u}' + \mathbf{M}' \tag{5}$$

$$\frac{D\theta'}{Dt} = -\mathbf{u}\cdot\nabla\theta_e + F_\theta \tag{6}$$

The coupling of dynamics and thermodynamics manifests itself in two parts:

1. An additional buoyancy source from the deviations in water vapour and the cloud ice in Eq. (5) in the density potential temperature
2. An additional source term F_θ on the right hand side of Eq. (6) due to diabatic processes (phase changes etc.).

2.2 Box model

The (zero-dimensional) box model represents an air parcel which is moved in the vertical direction with a velocity $w = w(t)$, prescribed for the whole simulation time t_s. Here, we assume only adiabatic processes, i.e. the vertical velocity produces an adiabatic cooling (expansion) or warming (compression) for the background temperature T_e due to

$$\frac{dT_e}{dt} = \frac{dT_e}{dz}\cdot\frac{dz}{dt} = -\frac{g}{c_p}\cdot w(t) \tag{7}$$

The governing equations for the dynamics reduce to

$$\frac{\partial\theta'}{\partial t} = F_\theta \tag{8}$$

i.e. the coupling of dynamics and thermodynamics is reduced to the additional diabatic forcing term. As indicated above, for consistency with the formulation of the dynamics of EULAG we have formulated the box model using environmental states T_e, p_e, θ_e, i.e. the model is formulated in perturbation form: All diabatic processes will only change $\theta' = \theta - \theta_e$, the adiabatic processes change the environment, i.e. T_e, p_e while θ_e remains constant. This concept can also be used for the dynamical model EULAG, where we can simulate adiabatic cooling due to upward motion by changing the background physical temperature T_e.

3 Model description – ice microphysics

In this section the newly developed ice microphysics scheme is described. First, we define the set of variables and derive the governing equations. The classes of aerosol and ice crystals will be defined, as well as their properties and mass (or size) distribution types. The moments of these distributions will be used in the microphysical equations. Finally, the currently implemented microphysical processes (nucleation, deposition, sedimentation) are described in detail. For all quantities we use SI units.

Aggregation is not yet implemented in the microphysics scheme. However, aggregation is of less importance for the cold temperature regime ($T < -40$°C) and/or for moderate vertical velocities (Kajikawa and Heymsfield, 1989). The development of an appropriate parameterisation consistent with the two-moment scheme is subject to ongoing research.

3.1 General assumptions and equations for ice microphysics

3.1.1 Prognostic equations

As we are interested in particular in the interplay of various competing nucleation modes acting in a cirrus cloud (in particular homogeneous vs. heterogeneous nucleation), we allow a non-specified number of aerosol and ice classes. Each aerosol class corresponds to an ice class that it nucleates and vice versa. Each class has a number and a mass concentration, N_x and q_x, respectively, which are the zeroth and first moments of a mass distribution $f(m)$. Note that N_x is meant in a mass specific sense, that is, the unit of the number concentration is kg^{-1} (per kg of dry air). We use this convention to be consistent with the formulation of the advection equations in flux form. This formulation will be used for the sedimentation of ice crystals, see below. However, ice crystal number densities and ice water content can be derived using the ambient density ρ: $n_c = N_c\cdot\rho$, IWC $= q_c\cdot\rho$. The kind of the distribution is preselected (e.g. log-normal or gamma etc.). The moments of $f(m)$ are

$$\mu_k[m] := \int_0^\infty f(m)\, m^k\, dm, \quad k\in\mathbb{R}_{\geq 0} \tag{9}$$

with the normalisation $\mu_0=N_x$. Prognostic equations for the number and mass concentrations of each aerosol and ice class form the basis of our bulk microphysical two-moment scheme.

Note that we prefer mass distributions whereas observers present their measurements usually as size distributions. Ice crystals in nature appear in a myriad of shapes. Crystal mass is therefore a more convenient choice for model formulation than crystal size. Therefore we formulate the prognostic equations for masses; sizes and shapes are diagnosed from them.

Ice crystal shape is important for depositional growth (Stephens, 1983), sedimentation (Heymsfield and Iaquinta, 2000) and radiative properties (Wendisch et al., 2005, 2007) of ice crystals. The ice crystal shape depends clearly on temperature and ice supersaturation (e.g. Bailey and Hallet, 2004; Libbrecht, 2005) but columns seem to be a frequent habit below -40°C in a variety of field measurements (Heymsfield and McFarquhar, 2002, their Table 4.1). Therefore we assume columnar ice crystals in our model.

One essential difference of our scheme to other schemes (e.g. Kessler, 1969; Seifert and Beheng, 2005) is that we do not differentiate ice classes according to their size. Traditionally, cirrus ice was classified as cloud ice and snow, where cloud ice consisted of ice crystals that are so small that their terminal fall speed could be set to zero, while snow was the ice fraction that had non-negligible fall speeds. This classification allowed a better treatment of sedimentation in single-moment models. As a two-moment model partly overcomes the problems with sedimentation by introducing two sedimentation fluxes, for number and mass concentration, respectively, we no longer differentiate between cloud ice and snow. Instead our ice classes correspond to various nucleation processes (or to the respective aerosol class).

The processes ice crystal nucleation, depositional growth/sublimation and sedimentation are currently implemented in the scheme. The prognostic equations for potential temperature and the microphysical variables for n classes of ice (index c) and aerosol (index a) are thus:

$$\frac{D\theta}{Dt} = \frac{L\,\theta_e}{c_p\,T_e}(\mathrm{NUC}+\mathrm{DEP}) + D_\theta \tag{10}$$

$$\frac{Dq_v}{Dt} = -(\mathrm{NUC}+\mathrm{DEP}) + D_{q_v} \tag{11}$$

$$\frac{Dq_{c,j}}{Dt} = \frac{1}{\overline{\rho}}\frac{\partial(\overline{\rho} q_{c,j} v_{m,j})}{\partial z} + \mathrm{NUC_j} + \mathrm{DEP_j} + D_{q_{c,j}} \tag{12}$$

$$\frac{DN_{c,j}}{Dt} = \frac{1}{\overline{\rho}}\frac{\partial(\overline{\rho} N_{c,j} v_{n,j})}{\partial z} + \mathrm{NNUC_j} + \mathrm{NDEP_j} + D_{N_{c,j}} \tag{13}$$

$$\frac{Dq_{a,j}}{Dt} = \mathrm{NUCA_j} + \mathrm{DEPA_j} + D_{q_{a,j}} \tag{14}$$

$$\frac{DN_{a,j}}{Dt} = -\mathrm{NNUC_j} + \mathrm{NDEP_j} + D_{N_{a,j}} \tag{15}$$

where j is the respective class index and

$$\mathrm{NUC} = \sum_{j=1}^{n} \mathrm{NUC_j},\ \mathrm{DEP} = \sum_{j=1}^{n} \mathrm{DEP_j}. \tag{16}$$

Here, θ denotes potential temperature, T_e and θ_e denote the physical and potential temperature of the environmental state, respectively. L_s is the latent heat of sublimation, c_p denotes the specific heat at constant pressure and $\overline{\rho}$ denotes the density of the reference state. q_v is the specific humidity. D_ψ terms represents sources and sinks of the model variable ψ due to processes not explicitely represented in the equations (e.g. turbulent transport, diffusion etc.). $v_{m,j}$ and $v_{n,j}$ are the mass and number weighted terminal velocities (see Sect. 3.4), respectively. The terms NUC_j and NNUC_j represent the sources and sinks for the ice crystal mass and number concentration, respectively, due to nucleation. Sources and sinks related to diffusional growth or sublimation are represented by the terms DEP and NDEP. We assume that every ice crystal nucleates from an aerosol particle (for both nucleation types, heterogeneous and homogeneous), hence the aerosol particle will be removed (i.e. it is now inside the crystal) from the aerosol number concentration and it will be released if the ice crystal sublimates completely. Therefore we can treat the sources and sinks for the aerosol number concentration using the same terms NNUC_j and NDEP_j. For treating the sources and sinks of the aerosol mass concentration we use the terms NUCA_j and DEPA_j. Note, that there is no sedimentation of the aerosol particles (due to their small masses).

3.1.2 Crystal shape and mass-size relation

For parameterisation of the various processes we need assumptions on the properties of single ice crystals, for instance their shapes. Generally, we assume that ice crystals are hexagonal columns (Bailey and Hallet, 2004), with height L and diameter D (twice the side length of the hexagon). The aspect ratio $r_a := L/D$ depends on crystal size, such that small crystals have $r_a=1$ and larger crystals have $r_a>1$. Mass-length relations from Heymsfield and Iaquinta (2000) of the form $L(m)=\alpha(m)\,m^{\beta(m)}$ with piecewise constant parameter functions $\alpha(m)$, $\beta(m)$ (Table 1) are used to derive crystal size from the prognostic quantity crystal mass. The bulk ice density is assumed as $\rho_b=0.81\cdot 10^3\,\mathrm{kg\,m^{-3}}$ (Heymsfield and Iaquinta, 2000). The parameter values are such that the boundary between small and large crystals is $m_t=2.146\cdot 10^{-13}$ kg, or equivalently $L_t=7.416$ μm. The aspect ratio can be formulated as a function of m; using the formula for the volume of a hexagonal column ($V=(\sqrt{27}/8)\cdot D^2\cdot L$) and the mass-length relations we arrive at:

$$r_a(m) = \begin{cases} 1 & \text{for } m < m_t \\ \sqrt{\frac{\sqrt{27}\rho_b}{8\alpha^{\frac{3}{\beta}}}}\cdot m^{\frac{3-\beta}{2\beta}} & \text{for } m \geq m_t \end{cases} \tag{17}$$

Table 1. Values for α, β in the general mass-length relation; here, m_t=2.146 · 10^{-13} kg denotes the transition between aspect ratio r_a=1 and r_a>1, this ice crystal mass is equivalent to a ice crystal length of L_t=7.416μm

m	$\alpha(m)^{-1}$	$\beta(m)^{-1}$
$m<m_t$	526.1	3.0
$m>m_t$	0.04142	2.2

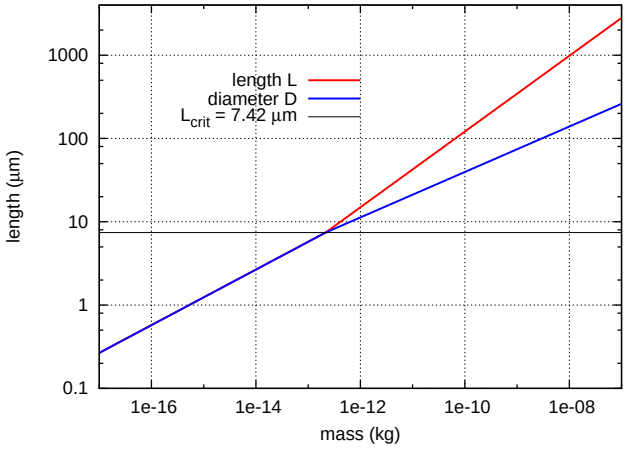

Fig. 1. Length (L) and diameter (D) of hexagonal ice crystals as functions of the ice crystal mass m.

In Fig. 1 length and diameter of the ice crystals are shown as functions of crystal mass, and in Fig. 2 the aspect ratio vs. the ice crystal mass and length is shown.

3.1.3 Sedimentation and mass-fall speed relation

For formulating the sedimentation fluxes of the ice mass and number concentrations, we need assumptions on the terminal velocity of a single ice crystal. Here again we use an ansatz by Heymsfield and Iaquinta (2000): $v_0(L)$=$x \cdot L^y$.

Using the mass-length relations derived above we formulate the terminal velocity as a function of crystal mass:

$$v_0(m) = \gamma(m) \cdot m^{\delta(m)} \tag{18}$$

with piecewise constant parameter functions $\gamma(m)$, $\delta(m)$, as given in Table 2. The parameters have been derived using the coefficients for small columns by Heymsfield and Iaquinta (2000). The terminal velocities v_0 are valid for reference values of $T_{0,1}$=233 K, $p_{0,1}$=300 hPa, for other temperatures and pressures we apply the correction factor

$$c(T, p) = \left(\frac{p}{p_0}\right)^{-0.178} \left(\frac{T}{T_0}\right)^{-0.394}, \tag{19}$$

such that $v(m, T, p)$=$\gamma(m)\, m^{\delta(m)}\, c(T, p)$. For very large ice crystals (L>1899 μm) we use coefficients adapted from

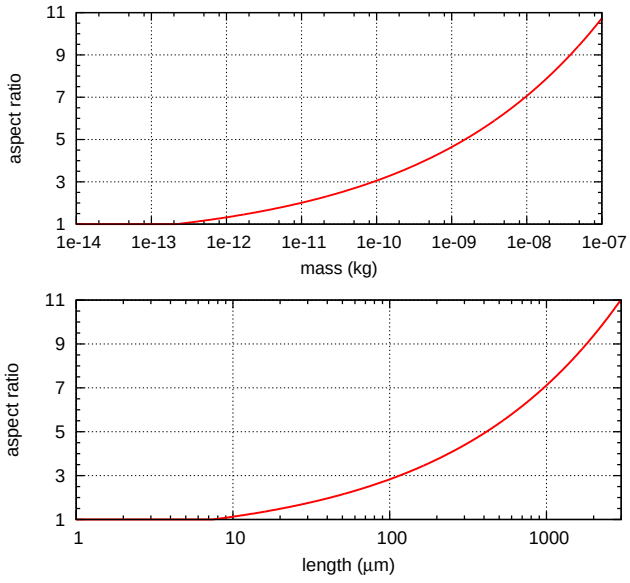

Fig. 2. Aspect ratio r_a of hexagonal ice crystals versus ice crystal mass m (upper panel) and length L (lower panel), respectively.

Table 2. Values for γ, δ in the velocity-mass Eq. (18); the transition masses are m_1=2.146 · 10^{-13} kg, m_2=2.166 · 10^{-9} kg, m_3=4.264 · 10^{-8} kg; equivalent lengths are L_1=7.416μm, L_2=490.0μm, L_3=1899μm

m	$\gamma(m)$	$\delta(m)$
$m \le m_1$	735.4	0.42
$m_1 \le m \le m_2$	63292.4	0.57
$m_2 \le m \le m_3$	329.8	0.31
$m_3 \le m$	8.8	0.096

Barthazy and Schefold (2006), who used a reference state of $T_{0,2}$=270 K, $p_{0,2}$=815 hPa. This second reference state was taken into account in the derivation of our coefficients, which are then valid for the whole tropospheric temperature and pressure range. The terminal velocity of a single ice crystal vs. its mass is shown in Fig. 3.

3.1.4 Choice of distribution type

For the formulation of the process rates in Eqs. (10–15) it is required to choose an a priori distribution type for the crystal masses and the masses of single aerosol particles. This choice can be handled very flexible (for instance as an entry in a FORTRAN namelist) when we are able to formulate the process rates in terms of general moments of the distribution. Then specification of a distribution in the model simply means branching into the corresponding function for the general moments. Because of this flexibility it does not matter

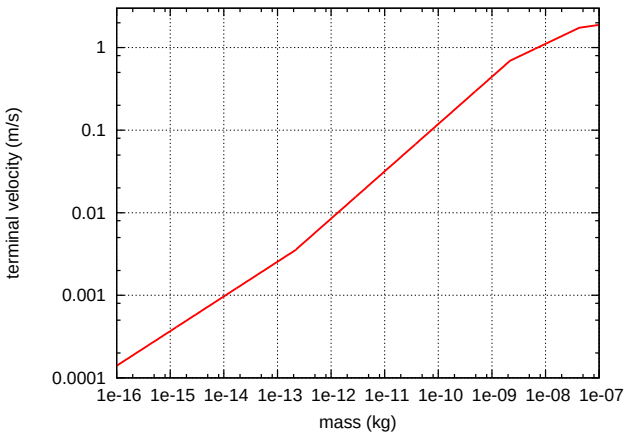

Fig. 3. Terminal velocity $v(m)$ of a single ice crystal as function of the crystal mass m.

much which kind of distribution we use here to derive the process rates. However, the model formulation is simpler when we select a lognormal distribution than when we select something else. The reason for that is the special form of the mass-size and mass-fall speed relations that we have assumed and that are common to cloud microphysics formulations at least since the 1970s. These relations have the form of a power law. It can easily be shown that when two quantities are related by such a power law and one quantity is lognormally distributed, then the other quantity is lognormally distributed as well. There are other distributions that have that property as well, e.g. Weibull and generalised gamma distributions. The former of these is a generalisation of the exponential distribution and might sometimes apply, e.g. for young contrails (Gierens, 1996). The latter has more parameters then the lognormal, which has two. Since it is difficult to derive equations for all parameters, one usually has to fix them somehow in an ad hoc way. Hence, we prefer to have a distribution with few parameters that avoids such procedures as much as possible. When a gamma distribution is selected for crystal sizes, as is often done, then masses and terminal velocities are generalised gamma distributed. However, from observations there is no evidence for preferring (generalised) gamma distributions against lognormal distributions for fitting size distributions of ice crystals. For many observational data, a lognormal distribution can be fitted as well as a generalised gamma distribution (M. DeReus, personal communication), and indeed, lognormal fits were used in several studies (e.g. Schröder et al., 2000)

Also the observation of multiple size modes does not call for multi-parameter distributions. We strongly believe that multiple modes are the result of mixing of ice crystal populations that have different origin. In our model such cases are covered by the use of multiple ice classes, where the combined size distribution of several classes will often show several modes. Hence, we prefer the lognormal distribution.

The lognormal distribution for the ice crystal mass can be written as

$$f(m) = \frac{N_c}{\sqrt{2\pi}\log\sigma_m} \cdot \exp\left(-\frac{1}{2}\left(\frac{\log\left(\frac{m}{m_m}\right)}{\log\sigma_m}\right)^2\right) \cdot \frac{1}{m} \quad (20)$$

with geometric mean mass m_m and geometric mass standard deviation σ_m. The lognormal distribution is completely specified once its zeroth, first, and second moment are given. The prognostic variables of the two-moment scheme let the second moment a free parameter that we either have to fix to a constant or to make a function of the mean mass. We use the latter possibility. For this purpose we follow Höller (1986) and define a "predominant mass": $m_{\mathrm{pre}} := \mu_2[m]/\mu_1[m]$, divide it by the mean mass $\overline{m} := \mu_1[m]/\mu_0[m]$ and set the ratio r_0 of these masses constant, that is:

$$r_0 := \frac{m_{\mathrm{pre}}}{\overline{m}} = \frac{\mu_2[m]\mu_0[m]}{\mu_1[m]^2} = \exp\left((\log(\sigma_m))^2\right). \quad (21)$$

Hence, the geometric standard deviation can be expressed as

$$\sigma_m = \exp\left(\sqrt{\log r_0}\right) \text{ or } \log\sigma_m = \sqrt{\log r_0} \quad (22)$$

Using Eq. (22) the analytical expression for the moments of the lognormal distribution $f(m)$ can be written as follows:

$$\mu_k[m] = N_c \cdot m_m^k \exp\left(\frac{1}{2}(k\log(\sigma_m))^2\right) \quad (23)$$

$$= N_c \cdot m_m^k r_0^{\frac{k^2}{2}} = N_c \cdot \overline{m}^k r_0^{\frac{k(k-1)}{2}} \quad (24)$$

Obviously the formulation using the ratio r_0 is much simpler than the formulation using σ_m.

Given the lognormal mass distribution, the corresponding lognormal distributions for the related quantities size and fall speed are obtained using the following transformation (e.g. for crystal length L):

$$L_m = \alpha \cdot m_m^\beta, \quad \log(\sigma_L) = \beta \cdot \log(\sigma_m) \quad (25)$$

Here we have considered the parameters as constant for the sake of simplicity. Since the coefficients are actually piecewise constant functions of mass, the transformation formula above is not strictly correct. One possible correction is the use of truncated moments (see below).

In Table 3 the values of σ_m and σ_L depending on the ratio r_0 and the mass range are shown.

3.2 Nucleation

Two different nucleation processes are parameterised in our scheme: First, homogeneous freezing of supercooled aqueous solution droplets (Sect. 3.2.1) and second, heterogeneous freezing on solid aerosol particles (Sect. 3.2.2). Both mechanisms depend on relative humidity wrt ice; for calculating relative humidities from prognostic variables (temperature, specific humidity, pressure), we use formulae from Murphy and Koop (2005) for the saturation pressures of (supercooled) water and ice.

Table 3. Geometric standard deviations σ_m and σ_L, depending on the ratio r_0. The transition mass m_t=2.146 · 10^{-13} kg is equivalent to a length of L_t=7.416μm.

r_0	σ_m	σ_L	
		$m<m_t$	$m>m_t$
1.25	1.60	1.17	1.24
1.50	1.90	1.24	1.34
2.00	2.23	1.32	1.46
3.00	2.85	1.42	1.61
4.00	3.25	1.48	1.71
6.00	3.81	1.56	1.84
8.00	4.23	1.62	1.92
16.0	5.29	1.74	2.13

3.2.1 Homogeneous nucleation

The solute mass (mass of H_2SO_4) in a solution droplet is equivalent to the radius r of a sphere of the pure solute. For this radius we prescribe a lognormal size distribution $f(r)$ with the geometric mean radius r_m and a geometric standard deviation σ_r.

Given the solute mass, the radius r_d of the solution droplet is obtained from the Köhler theory, depending on temperature and relative humidity. From the Köhler theory in its simplest form we know that at (water) saturation the equilibrium droplet radius r_d is proportional to the square root of the solute mass, i.e. proportional to $r^{3/2}$, a power law relationship. Hence the solution droplets are approximately lognormally distributed as well, which is in accordance to measurements of upper tropospheric aerosol (Minikin et al., 2003).

The probability for an aqueous H_2O/H_2SO_4 solution droplet of volume V_d to freeze within a time period Δt is

$$P(\Delta a_w, T, \Delta t) = 1 - \exp\left[-J_{hom}(\Delta a_w, T) V_d(T) \Delta t\right] \quad (26)$$

where $J_{\mathrm{hom}}(\Delta a_w, T)$ denotes the homogeneous nucleation rate which is parameterised according to Koop et al. (2000) in terms of temperature and $\Delta a_w := a_w - a_w^i$, the difference of water activity in the solution and a_w^i, the activity of the water in the solution in equilibrium with ice at temperature T (i.e. $a_w^i = e_i^*(T)/e_w^*(T)$, the ratio of the saturation vapour pressures wrt ice and liquid water, respectively). a_w^i is thus a function of temperature alone. The water activity itself is the ratio of the equilibrium vapour pressure over the solution to the equilibrium vapour pressure over pure liquid water.

When dynamical processes (uplift) are slow enough that solution droplets can equilibrate their volume to changes in relative humidity, then the water activity equals the saturation ratio (wrt water). This is assumed here. Hence, the homogeneous nucleation rate J_{hom} can be expressed as a function of relative humidity and the temperature. The number of ice crystals created within a time step Δt from an initial aerosol concentration N_a can now be calculated as

$$\Delta N_c = N_a \int_0^\infty f_a'(r) P(\Delta a_w, T, \Delta t)\, dr \quad (27)$$

(where $f_a'(r)$ is the aerosol size distribution normalised to 1) and the frozen ice water content can be calculated as

$$\Delta q_c = N_a \int_0^\infty f_a'(r)(r) w_w \rho_d V_d P(\Delta a_w, T, \Delta t)\, dr \quad (28)$$

where w_w denotes the H_2O weight fraction and ρ_d the density of the solution, respectively. Exploiting the lognormal character of the dry aerosol size distribution, we can use a Gauss-Hermite integration for numerical calculation of the integral (Gierens and Ström, 1998). The integral in Eq. (28) is usually much less than one, so that homogeneous nucleation usually is not number limited. Note, that homogeneous freezing of solution droplets only occurs at $T<-38$°C, i.e. below the supercooling limit of pure water.

Formation of ΔN_c ice crystals simply implies loss of $\Delta N_a = -\Delta N_c$ aerosol particles. However, a priori it is not clear how much aerosol mass is transferred to the ice in the nucleation process. Here we use the following procedure. While the aerosol number concentration decreases by a factor $f_n = |\Delta N_a|/N_a$ the dry aerosol mass concentration in the aerosol class decreases by a factor f_m. Hence the mean dry aerosol mass is reduced by a factor $(1-f_m)/(1-f_n)$. We can compute and apply this factor once a relation between f_m and f_n is given. For this we make the ansatz

$$f_m^\alpha = f_n. \quad (29)$$

The postulate $\alpha \geq 1$ expresses that fact that large droplets (consisting of large aerosols) will freeze first and vanish from the aerosol pool (see e.g. Haag et al., 2003a, Fig. 8). It turns out from additional calculations, that a factor α=1.33 is a good approximation. We will use the same approach for the sublimation of ice crystals, see Sect. 3.3. Note that we let the width parameter (σ_m) of the aerosol mass distribution unchanged during the nucleation event.

The shift of the mean mass of the background aerosol distribution is optional and can be switched on and off. For very large background aerosol concentrations, the shift of the mean mass is marginal and can be switched off. Then, only the number concentration is decreased, while the mean mass or size of the aerosol distribution remains constant; the new mass distribution is calculated using the new number concentration. For simulations with high vertical velocities at very cold temperatures ($T<210$ K) the shift of the mean mass is recommended.

The impact of shifting the modal radius of the background aerosol distribution leads to smaller radii of solution droplets during the ongoing nucleation event, resulting in a decrease of number density of nucleated ice crystals due to the abrupt change during a nucleation event.

3.2.2 Heterogeneous nucleation

Although the investigation of different nucleation mechanisms within the same environment is one of the key issues which will be studied using the new cirrus microphysics, we mention heterogeneous nucleation only briefly here, because we will not use it further in the present paper. Generally, the parameterisation for heterogeneous nucleation makes use of prescribed background aerosols, which act as ice nuclei. Thus, there is an explicit impact of the aerosol on the formation of ice crystals and also washout of the background aerosol trapped in the sedimenting ice crystals is described. After nucleation the aerosol particles are trapped inside the ice crystals and are released as soon as the ice crystals evaporate.

In our model we can use parameterisations of heterogeneous nucleation of any type, more or less sophisticated. In Part 1b (Spichtinger and Gierens, 2009) we will extensively use heterogeneous and homogeneous nucleation within the same environment; the parameterisation that is used is described there.

3.3 Deposition growth and sublimation

The growth Eq. (see e.g. Stephens, 1983) for a single ice crystal of mass m reads:

$$\frac{dm}{dt} = 4\pi C D_v f_1 f_2 \left[\rho_v(T_e) - \rho_{s,i}(T_s)\right] \tag{30}$$

where $\rho_v(T_e)$ and $\rho_{s,i}(T_s)$ denote the ambient water vapour density, derived from ambient humidity and temperature T_e and the saturated (with respect to ice) water vapour density at the ice crystal surface, i.e. at surface temperature T_s. The other factors in Eq. (30) are as follows:

– Diffusivity of water vapour in air

$$D_v = 2.11 \cdot 10^{-5} \left(\frac{T}{T_0}\right)^{1.94} \left(\frac{p_0}{p}\right) \mathrm{m^2 s^{-1}} \tag{31}$$

according to Pruppacher and Klett (1997) using reference values T_0=273.15 K and p_0=101325 Pa, respectively.

– Capacitance factor C which accounts for the non-spherical crystal shape. We could have used the capacitance factors for hexagonal columns of Chiruta and Wang (2005) here, but we did not for the following reasons: First, the well-known uncertainty in the deposition coefficient (see below) has a larger effect on the results than the choice of C. Second, the formulation of ventilation factors (see below) has been derived for spherical water drops and only few experiments have been carried out for other shapes than spherical Hall and Pruppacher (1976). Third, an ice cloud contains anyway a mixture of crystal shapes and habits. Inclusion of the correct capacitance factor for one habit leads to inconsistencies with other habits. For these reasons we simply followed Hall and Pruppacher (1976). For spheres of radius r, C=r. Hexagonal columns with length L=2a and diameter D=2b can be approximated by prolate spheroids with semi axes a and b ($a \geq b$), i.e. with an aspect ratio r_a=L/D=a/b. The capacitance factor C can be determined using the electrostatic analogy (McDonald, 1963)

$$C = \frac{L\epsilon'}{\log\left(\frac{1+\epsilon'}{1-\epsilon'}\right)} = \frac{A'}{\log\left(\frac{a+A'}{b}\right)} \tag{32}$$

where ϵ'=$\sqrt{1-(b/a)^2}$=$\frac{1}{a}\sqrt{a^2-b^2}$=$\frac{A'}{a}$ denotes the eccentricity of the spheroid. We use the aspect ratio r_a introduced in Sect. 3.1 for our calculations.

– Correction factor f_1 for the difference between the transfer of water molecules to the crystal by pure diffusion and that according to kinetic treatment of individual water molecules (important for very small crystals with sizes less than 1 μm):

$$f_1 = \frac{r^*}{r^* + l_M^*}, \text{ with} \tag{33}$$

$$r^* = \frac{A}{4\pi C}, \quad l_M^* = \frac{2\pi M_w}{R T_s} \frac{D f_2}{2\alpha_d (2-\alpha_d)^{-1}} \tag{34}$$

where A is the surface area of the ice crystal, M_w denotes molecular weight of water and R is the universal gas constant. α_d denotes the deposition coefficient. Currently there is no agreement on a generally accepted value of α_d. Measured values range between $0.004 \leq \alpha_d \leq 1$ (see e.g. Pruppacher and Klett, 1997; Magee et al., 2006), however most models work well with $\alpha_d \geq 0.1$ (Lin et al., 2002) for reasons discussed in Kay and Wood (2008). The deposition coefficient could even depend on crystal size (e.g. Gierens et al., 2003) or on ice supersaturation (Wood et al., 2001). For our validation runs we have set α_d=0.5 (see e.g. Kärcher and Lohmann, 2002a,b).

– Ventilation factor f_2 to correct for the enhanced growth of ice crystals due to enhanced water vapour flux arising from motion of the crystal relative to the environmental air (important for large crystals). We follow Hall and Pruppacher (1976) and set:

$$f_2 = \begin{cases} 1 + 0.14 (N_{Sc}^{\frac{1}{3}} N_{Re}^{\frac{1}{2}})^2 & \text{for } N_{Sc}^{\frac{1}{3}} N_{Re}^{\frac{1}{2}} \leq 1 \\ 0.86 + 0.28 (N_{Sc}^{\frac{1}{3}} N_{Re}^{\frac{1}{2}}) & \text{for } N_{Sc}^{\frac{1}{3}} N_{Re}^{\frac{1}{2}} > 1 \end{cases} \tag{35}$$

where N_{Sc}=$D\eta/\rho$ denotes the Schmidt number, η is the viscosity of air and N_{Re} is the Reynolds number defined by characteristic dimensions of the ice crystal.

The latent heat released on the growing crystal must be diffused to the ambient air. This is described by an analogous equation:

$$L_s \frac{dm}{dt} = 4\pi C D_v f_1^* f_2^* (T_e - T_s) \tag{36}$$

L_s denotes the latent heat of sublimation, the coefficients f_1^*, f_2^* are the counterparts to those in Eq. (30):

– $f_1^* = \frac{r^*}{r^* + l_Q^*}$ with $l_Q^* = \frac{K f_2^*}{\frac{1}{\rho_a^4} \overline{u_r} \beta_d c_p}$.
Here, K is the thermal conductivity of moist air, $\overline{u_r}$ is the average thermal velocity of air molecules striking the ice surface and β_d=1 is the thermal accommodation coefficient.

– The ventilation factor f_2^* for thermal diffusion is calculated as follows (Hall and Pruppacher, 1976):

$$f_2^* = \begin{cases} 1.00 + 0.14\chi_Q^2 & \text{for } \chi_Q < 1 \\ 0.86 + 0.28\chi_Q & \text{for } \chi_Q > 1 \end{cases}, \tag{37}$$

$\chi_Q = N_{Pr}^{\frac{1}{3}} N_{Re,l_Q^*}^{\frac{1}{2}}$, where N_{Pr} denotes the Prandtl number and N_{Re,l_Q^*} denotes the Reynolds number for the characteristic length l_Q^*.

In order to compute the parameters required for a parameterisation, the two diffusion equations are solved iteratively using a fourth order Runge-Kutta scheme. For crystals of intermediate size, i.e. above the kinetic regime but still small enough such that ventilation is negligible, the ansatz by Koenig (1971) $\frac{dm}{dt} \approx a m^b$, provides a good approximation to the numerical solution. The coefficients a, b depend on saturation ratio, temperature and pressure and can be derived using a least squares regression of exponential type $f(x) = ax^b$. The coefficients a, b have been calculated for pressures in the range $150 \le p \le 600$ hPa in 50 hPa bins and for the temperature range $-80 \le T \le -20$°C in 1 K bins. For the Runge-Kutta integration we have assumed water saturation. The actual value of a during a simulation is the product of the tabulated value and $(e - e_i^*)/(e - e_w^*)$. This factor is negative for ice-subsaturated conditions, i.e. the equations then describe crystal sublimation. The functions $a(p, T)$ and $b(p, T)$ for selected pressures are displayed in Fig. 4. The form of the Koenig approximation makes it ideal for later use in the prognostic equation for q_c. However, it overestimates strongly the crystal growth in the kinetic regime and underestimates the influence of the ventilation factor for large crystals. In order to overcome these problems, we introduce a correction of the following form:

$$\frac{dm}{dt} \approx \begin{cases} a \cdot m^b \cdot \left(1 - \exp\left(-\left(\frac{m}{m_0}\right)^\gamma\right)\right) & \text{for } m < m_l \\ a \cdot m^b \cdot \left(\frac{m}{m_l}\right)^\delta & \text{for } m \ge m_l \end{cases} \tag{38}$$

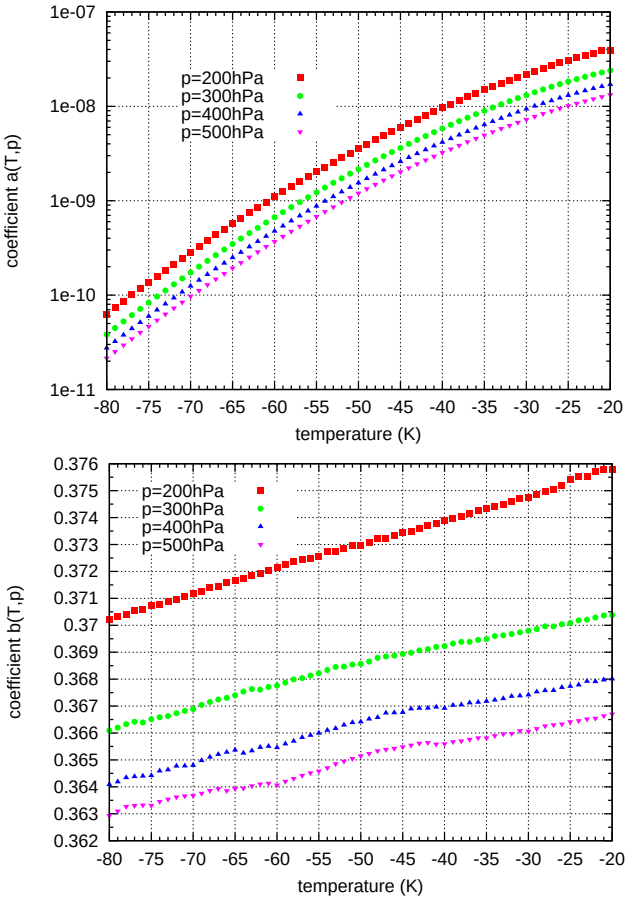

Fig. 4. Coefficients $a(p, T)$ (top) and $b(p, T)$ (bottom) for Koenig's ansatz $dm/dt \approx a(p, T) m^{b(p,T)}$ and the approximation of the numerical solution of Eq. (30) for different pressures.

where $m_0 = m_0(p, T) \sim 10^{-16} - 10^{-14}$ kg, $\gamma = \gamma(p, T) \sim 0.2 - 0.25$, $m_l = 2.2 \cdot 10^{-10}$ kg, and δ=0.12.

Using these corrections we are able to approximate the mass growth rates for single crystals within an error margin of less than 5% compared to the numerical solution.

The numerical solutions together with the original Koenig ansatz and the new approximations are shown in Fig. 5.

Now we are going to derive the "integrated" equation for the cloud ice mixing ratio tendency:

$$\frac{dq_c}{dt} = \frac{d}{dt} \int_0^\infty f(m)\, m\, dm \tag{39}$$

We may interchange the derivative with integration, invoke the product rule and arrive at:

$$\frac{dq_c}{dt} = \int_0^\infty \frac{\partial f(m)}{\partial t} m\, dm + \int_0^\infty f(m) \frac{\partial m}{\partial t}\, dm$$

The second integral vanishes, since $\partial m/\partial t \equiv 0$ (because m must be interpreted here a co-ordinate in m-space, and the co-ordinate system is, of course, fixed). The first integral can be

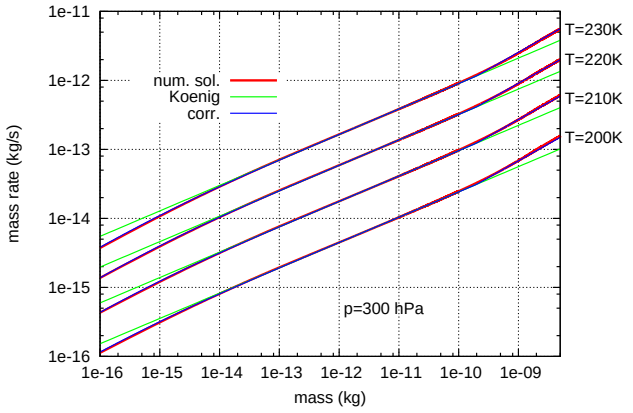

Fig. 5. Growth rates dm/dt of single ice crystals vs. crystal mass. Results of the numerical integration (red) and approximations using the original Koenig ansatz (green) and the Koenig ansatz with our corrections (blue) for various temperatures (T=230/220/210/200 K) and fixed pressure (p=300 hPa).

cast into another form when we make use of the "continuity equation" in mass-space, which reads

$$\frac{\partial f(m)}{\partial t} + \frac{\partial}{\partial m}\left(\frac{dm}{dt} f(m)\right) = 0. \tag{40}$$

Inserting this into the first integral above, we find

$$\frac{dq_c}{dt} = -\int_0^\infty m \frac{\partial}{\partial m}\left(\frac{dm}{dt} f(m)\right) dm.$$

Partial integration yields

$$\frac{dq_c}{dt} = -\left[m \frac{dm}{dt} f(m)\right]_0^\infty + \int_0^\infty \frac{dm}{dt} f(m)\, dm,$$

where the integrated part in the square brackets vanishes, because $f(m)$ vanishes at infinity, and at the lower boundary m=0. Finally, we arrive at the following simple expression:

$$\frac{dq_c}{dt} = \int_0^\infty \frac{dm}{dt} f(m)\, dm.$$

Here, $\frac{dm}{dt}$ can be interpreted as the "advection velocity" in the "mass"-space due to crystal growth; hence, we can insert the modified Koenig approximation from above. Let us first treat the case where the largest crystals are still smaller than m_l (i.e. $f(m) \approx 0$) for $m > m_l$). This gives

$$\begin{aligned}\frac{dq_c}{dt} &= \int_0^\infty f(m) a \cdot m^b \left(1 - e^{-\left(\frac{m}{m_0}\right)^\gamma}\right) dm \qquad (41)\\ &= \int_0^\infty f(m) a \cdot m^b dm \\ &\quad - \int_0^\infty f(m) a \cdot m^b e^{-\left(\frac{m}{m_0}\right)^\gamma} dm \\ &= a\mu_b[m] - a \int_0^\infty f(m) m^b e^{-\left(\frac{m}{m_0}\right)^\gamma} dm \qquad (42)\end{aligned}$$

The original Koenig approximation results into an ice water mass rate of $a\mu_b[m]$. Additional numerical integrations and our simulations showed that we can approximate the integral in Eq. (42) so that for sufficiently small crystals the tendency for q_c can be cast into the following form:

$$\frac{dq_c}{dt} \approx a \cdot \mu_b[m] \cdot \left(1 - \exp\left(-\left(\frac{\overline{m}}{m_0 \cdot \chi}\right)^\gamma\right)\right) \tag{43}$$

where $\chi \approx 20$. Hence, we simply need another correction factor. It turns out that this correction will only have an impact for low temperatures and high vertical velocities (see below).

For large crystals, the ventilation correction becomes important. These crystals alone give the following contribution:

$$\frac{dq_c}{dt} = \int_{m_l}^\infty f(m) a \cdot m^b \cdot \left(\frac{m}{m_l}\right)^\delta dm \tag{44}$$

which can be computed using known expressions for truncated moments (Jawitz, 2004). Finally, we arrive at the following expression:

$$\frac{dq_c}{dt} \approx a\,\mu_b[m] \begin{cases} \left(1 - e^{\left(-\left(\frac{\overline{m}}{m_0 \cdot \chi}\right)^\gamma\right)}\right) & \text{for } \overline{m} \le m_l \\ \left(\frac{\overline{m}}{m_l}\right)^\delta & \text{for } \overline{m} > m_l \end{cases} \tag{45}$$

Note that $\frac{dq_c}{dt}$ is expressed using the mean mass (first moment) and the moment of order b of the mass distribution. This formulation makes it possible to use any kind of mass distribution for which analytical expressions for the moments are known.

Growth of ice crystals does not affect their number concentration (as long as there is no aggregation), but sublimation does when the smallest ice crystals sublimate completely while larger crystals only loose some mass. We parameterise this effect in a simple way. Let the ice mass mixing ratio in a certain grid box be reduced by a fraction f_q during one time step. Then we assume that the corresponding fractional reduction of number concentration is given by $f_N = f_q^\alpha$, with $\alpha > 1$. This relation implies that when a small mass fraction sublimates, this is mainly due to shrinking of big crystals; when a large mass fraction vanishes, then also a large fraction of crystal number concentration must vanish. In the limiting cases, f_q=0 or f_q=1, we also have f_N=0 or f_N=1, respectively, as it should be. From numerical studies we found that α=1.1 produces plausible results. This value is in agreement with Harrington et al (1995), who derived from numerical simulations a range $1 \le \alpha \le 1.5$.

3.4 Sedimentation of ice crystals

From our parameterisation of the terminal velocity of a single ice crystal we derive terminal velocities for the mass and number concentrations, respectively. To this end let us consider the sedimentation fluxes of mass and number

concentrations:

$$\mathfrak{F}_m := \int_0^\infty \rho f(m) v(m) m \, dm \tag{46}$$

$$\mathfrak{F}_n := \int_0^\infty \rho f(m) v(m) \, dm \tag{47}$$

We use these definitions to define mass and number weighted terminal velocities, such that $\mathfrak{F}_m = \rho \, q_c \, v_m$, $\mathfrak{F}_n = \rho \, N_c \, v_n$. Hence:

$$v_m = \frac{1}{q_c} \int_0^\infty f(m) v(m) m \, dm \tag{48}$$

$$v_n = \frac{1}{N_c} \int_0^\infty f(m) v(m) \, dm \tag{49}$$

The terminal velocity of one single ice crystal is a function of its mass, viz. $v(m) = \gamma(m) \cdot m^{\delta(m)}$. For simplicity, let us first assume $\gamma(m) = \gamma_0$, $\delta(m) = \delta_0$ to be constants. This allows to simply express the mass and number weighted terminal velocities via the moments of $f(m)$:

$$v_m = \gamma_0 \cdot \frac{\mu_{\delta+1}}{\mu_1}, \quad v_n = \gamma_0 \cdot \frac{\mu_\delta}{\mu_0} \tag{50}$$

Actually, the coefficients in the mass vs. fall speed relation are piecewise constant, hence we can express the integrals by using truncated moments:

$$\int_0^\infty f(m) v(m) \, dm = \sum_{k=0}^{4} \int_{m_k}^{m_{k+1}} f(m) \gamma(m) m^{\delta(m)} dm = \sum_{k=0}^{4} \gamma(m) \mu_{\delta(m)}(m_k, m_{k+1}) \tag{51}$$

$$\int_0^\infty f(m) v(m) m \, dm = \sum_{k=0}^{4} \int_{m_k}^{m_{k+1}} f(m) \gamma(m) m^{\delta(m)+1} dm = \sum_{k=0}^{4} \gamma(m) \mu_{\delta(m)+1}(m_k, m_{k+1}) \tag{52}$$

where $\mu_k(m_l, m_u)$ denotes the k^{th} truncated moment with boundaries $m_l < m < m_u$. Here, $m_0 = 0$, $m_4 = \infty$, the values m_1, m_2, m_3 are given in Table 2. For the lognormal distribution the truncated moments can be expressed as follows (Jawitz, 2004):

$$\mu_k(m_l, m_u) = \mu_k[m] \frac{1}{\sqrt{\pi}} \int_{z(m_l)}^{z(m_u)} \exp(-z^2) dz \tag{53}$$

with the transformation

$$z(m) = \frac{\log\left(\frac{m}{m_m}\right) - k \log(\sigma_m)}{\sqrt{2}}, \tag{54}$$

For the calculation of the integral we have to evaluate the error function

$$\mathrm{erf(x)} = \frac{2}{\sqrt{\pi}} \int_0^x \exp(-r^2) dr \tag{55}$$

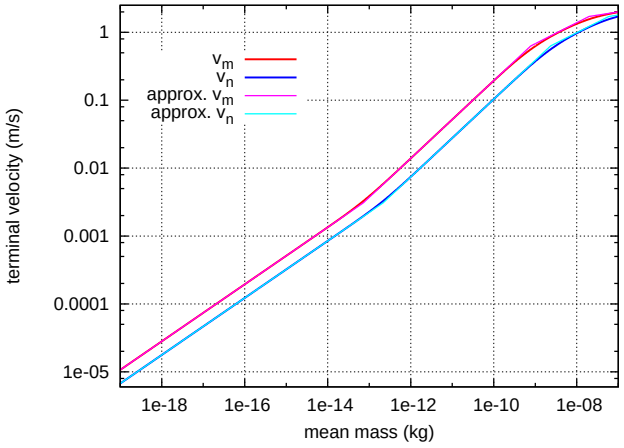

Fig. 6. Mean terminal velocities v_m, v_n for r_0=3 and the approximations by using the expressions of general moments as in Eq. (50) as piecewise constant functions.

In Fig. 6 the mean terminal velocities v_m, v_n for a typical value of r_0=3 (i.e. σ_m=2.852) are shown.

The treatment using truncated moments is computationally expensive. Therefore we approximate the analytical solutions by using general moments for different mass intervals of the curve, i.e.

$$v_m(m) \approx \gamma(m) \cdot \frac{\mu_{\delta(m)+1}}{\mu_1} \tag{56}$$

$$v_n(m) \approx \gamma(m) \cdot \frac{\mu_{\delta(m)}}{\mu_0} \tag{57}$$

The approximations are also shown in Fig. 6. Evidently, the approximation works rather well. Certain mathematical relations between moments (Lyapounov's inequality) guarantee that the ratio $v_m/v_n > 1$ for all $r_0 > 1$ which implies that the mass mixing ratio sediments faster than the number concentration, or in other terms, that large ice crystals fall faster than smaller ones.

The ratio v_m/v_n depends strongly on the width of the ice crystal mass distribution (parameter r_0). For too large values of r_0 a kind of decoupling of the variables N_c, q_c could be observed: The ice crystal number density concentrates in the upper layers of a cloud, while the cloud ice falls downwards very fast. This leads to unphysical behaviour, e.g. to extraordinary large ice crystals in the lower cloud levels and fall streaks. For realistic values of r_0 in the range $1 < r_0 \leq 4$ this does not occur.

In the EULAG model sedimentation is treated as a 1-D advection in vertical direction. Several advection schemes can be used: a simple implicit scheme or an explicit scheme (as used for the 3-D) with various orders and non-oscillatory option. In our studies we will usually use the explicit scheme of 2nd order (MPDATA) without the non-oscillatory option.

3.5 Microphysical time step

As we will see later in the validation section, the parameterisations can be sensitive to the prescribed time step. For box model calculations this is not a problem; the computational effort is so small, that we can easily use a very small time step. However, for the application of the microphysics scheme in a 2D/3D framework of the EULAG model the computational effort is much higher. For solving this problem, we implemented a so-called microphysical time step. Here, the "dynamical" time step, i.e. the time step for the dynamics in the EULAG model is split into a number of sub-time steps, i.e. $\Delta t_{mp} = \Delta t / n_{mp}$. There is an additional loop for each vertical column of n_{mp} sub time steps; here, only the microphysics (nucleation, growth/sublimation, sedimentation) is calculated. Then, the summed forcing terms from the sub-time steps are used for the next dynamical time steps. We use the microphysical time step adaptively: First, the forcings for a normal dynamical time step are calculated. If homogeneous nucleation takes place within this time step or the change in relative humidity wrt ice is larger than 1% due to deposition/sublimation, then the time splitting is used. We will see later in the validation of the nucleation parameterisation, which number of sub-time steps is appropriate.

4 Validation and discussion

The microphysics scheme is validated using two different types of comparisons. First, we use our microphysics in a box model setting to compare the ice crystal number densities that are nucleated homogeneously under a large variety of conditions with values derived from a box model with detailed ice microphysics scheme (Kärcher and Lohmann, 2002a,b). Additionally, some sensitivity studies are carried out. Second, we simulate a well-documented case of arctic cirrostratus and compare our results with 1-D simulations (Lin et al., 2005; Kärcher, 2005).

4.1 Comparison with detailed box model calculations

Kärcher and Lohmann (2002a) used a detailed box model (particle tracking, highly resolved aerosol size distribution) for testing an analytically derived relationship between the maximum possible ice crystal number density, formed by homogeneous nucleation, and vertical velocity. In our first step of validating the model, we carry out box model runs for the same conditions to compare ice crystal number densities with the results of Kärcher and Lohmann (2002a). The code of Kärcher and Lohmann (2002a) has been successfully applied to measurements of homogeneous nucleation in the large cloud chamber AIDA (Haag et al., 2003a) and to field measurements during INCA (Interhemispheric differences in cirrus properties from anthropogenic emissions, Gayet et al., 2006). So, our comparison with results of Kärcher and Lohmann (2002a) can be viewed as an indirect comparison with the AIDA and INCA results.

We use the following setup: We allow only homogeneous freezing and prescribe a constant vertical velocity in the range w=0.01−5.0 m s^{-1}. The initial conditions (p, T, q_v) are adapted such that temperature and pressure reach prescribed values $p\pm5$ hPa, $T\pm0.1$ K at the beginning of the homogeneous freezing event.

Initially we assume a very high aerosol number density so that nucleation is not constrained by the number of available nuclei. Later we will investigate cases with realistic background aerosol conditions, obtained from observations (e.g. Minikin et al., 2003). Within the box model framework we will also investigate the impact of pressure on the number density of ice crystals produced in the nucleation event.

4.1.1 Idealised simulations

In our first series of experiments we use only one class of (homogeneously formed) ice. The number density of the background aerosol is set to the very large value of N_a=10 000 cm^{-3}, such that nucleation cannot exhaust the background aerosol. Therefore we may safely neglect the shift in the mean mass of the aerosol size distribution. We choose a geometric standard deviation of σ_m=2.85 (r_0=3) for the lognormal distribution of the ice crystal mass. Additional sensitivity tests have been performed with r_0 in the range $2\leq r_0\leq 4$; these resulted in only slight variations compared to r_0=3. For a certain vertical velocity w we choose the time step such that the nucleation event is resolved: Δt=(0.05 m/w) (B. Kärcher, personal communication). The number of time steps is fixed at n_t=12 000.

We choose the same conditions (p, T) as in Kärcher and Lohmann (2002a), i.e. T=196, 216, 235 K and p=200 hPa, and a mean radius for the (dry) H_2SO_4 aerosol of r_m=25 nm. The reported values of temperature and pressure, respectively, in all boxmodel simulations refer always to the onset of homogeneous freezing. For investigating the effect of the width of the aerosol size distribution we vary the geometrical standard deviation: σ_r=1.3, 1.6, 1.9.

The results are shown in Fig. 7 in comparison with the values of Kärcher and Lohmann (2002a,b). The agreement between our results and those of the more detailed model is quite satisfying, in particular for the two higher temperatures. At the lowest temperature our model still produces results similar to those of Kärcher and Lohmann (2002a,b), but only up to w=10 cm s^{-1}. Generally we find from additional simulations (not shown) that the maximal vertical velocity at which our model produces reliable results decreases with decreasing temperature. At higher vertical velocities our model starts to underestimate the number of aerosols freezing, and the underestimation grows with the width of the aerosol size distribution. We believe that these errors have two sources.

The first error source is the assumption of equilibrium implicit in the Koehler equation and in the Koop

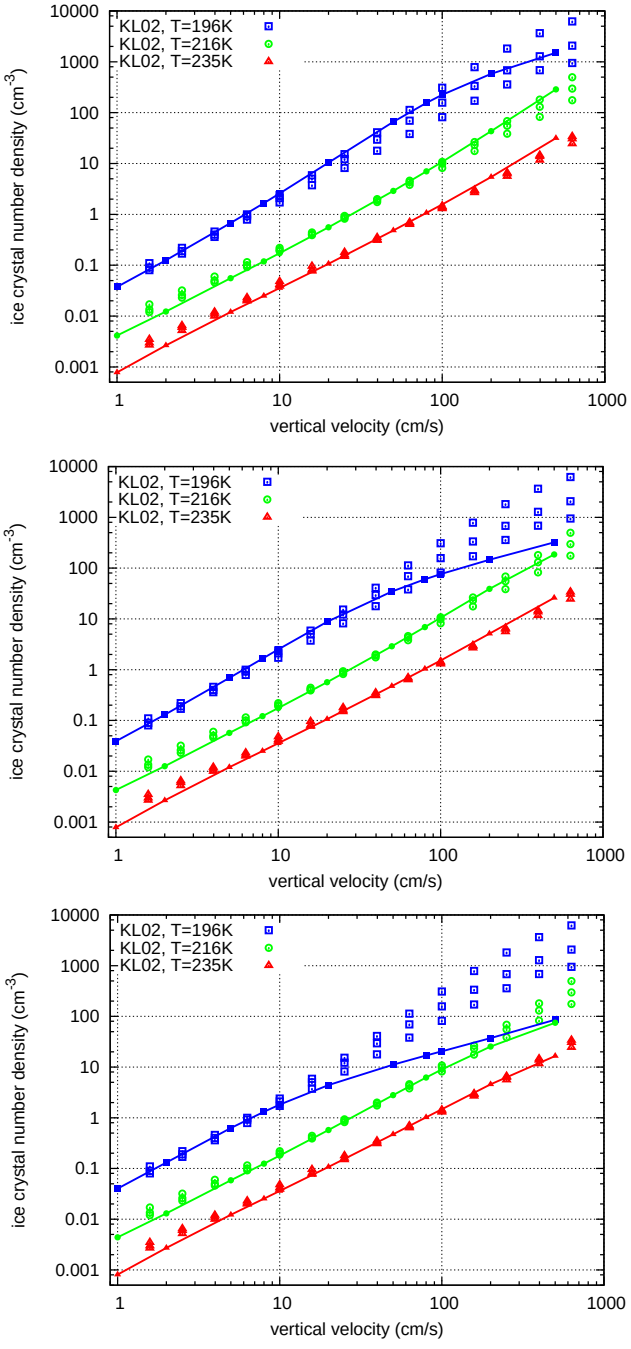

Fig. 7. Box model calculations for the homogeneously formed ice crystal number densities depending on the vertical velocity. The calculations for different temperatures are indicated by the colours (red: T=235 K, green: T=216 K, blue: T=196 K). Line points indicate calculations with our box model, points denotes values from Kärcher and Lohmann (2002a). The panels show the impact of the width of the aerosol distribution: top: σ_r=1.3, middle: σ_r=1.6, bottom: σ_r=1.9.

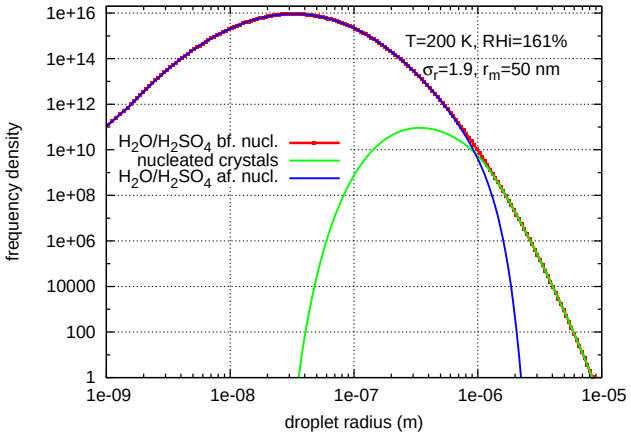

Fig. 8. Effect of a nucleation event during a time step of Δt=0.1 s at T=200 K and a relative humidity wrt ice RHi=161% for a quite broad aerosol distribution (r_m=50 nm, σ_r=1.9): The H_2O/H_2SO_4 droplet distribution before the nucleation event is indicated by the red line points, the green line indicates the distribution of freshly nucleated ice crystals and the blue line describes the H_2O/H_2SO_4 droplet distribution after the nucleation event.

parameterisation. Both the Koehler equation and the Koop parameterisation are based on the assumption of equilibrium, i.e. they are only strictly applicable when rates of water uptake on aerosol droplets are fast compared to the rate of change of saturation ratio. For high vertical velocities, especially in the low temperature range, this condition is not fulfilled. Hence, in a fast cooling environment the solution droplets are actually smaller than computed with the Koehler equation. The initial nucleation rate (when the threshold supersaturation is reached) is larger when the aerosol sizes are overestimated, first because of their increased volume, and second because of the overestimated water activity. However, the final number of ice crystals is the integral of $J_{\rm hom} V_d$ over time. Since the nucleation rate is initially overestimated, and since these crystals are too big, the initial crystal growth is overestimated as well, and so the initial depletion of excess vapour is overestimated. This can have two effects: First, the actual maximum supersaturation beyond the threshold is not reached in our model, hence maximum nucleation rates are underestimated. Second, the duration of the nucleation event is clipped. Overall, the time integral of $J_{\rm hom} V_d$ becomes underestimated, which is the effect that we see.

The solution of this problem requires introduction of prognostic equations for the aerosol dynamics, which currently is not part of our scheme.

The second error source works in a similar way, but it arises as an artifact of the assumptions required in a bulk model. When nucleation starts, it transforms the largest aerosol droplets into ice, cutting off the right tail of the droplet size distribution (see Fig. 8).

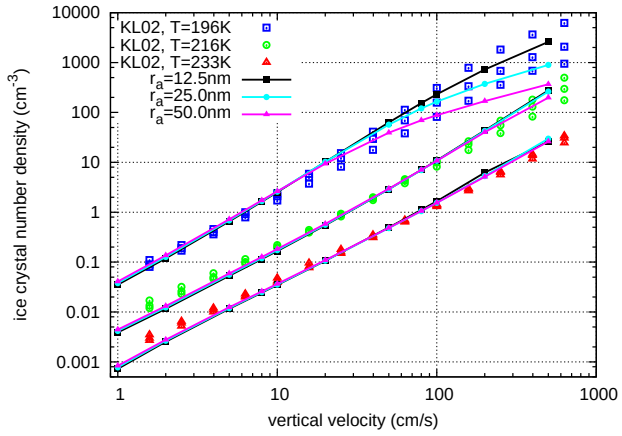

Fig. 9. Box model calculations for the homogeneously formed ice crystal number densities depending on the vertical velocity and on the temperature. For comparisons, the values from detailed microphysics calculations in Kärcher and Lohmann (2002a) are shown. For the simulations, we assume a fixed width for the aerosol distribution of σ_r=1.4. Here, the impact of geometric mean size of the aerosol distribution is shown: r_m=12.5 nm (black), r_m=25.0 nm (cyan), r_m=50.0 nm (magenta).

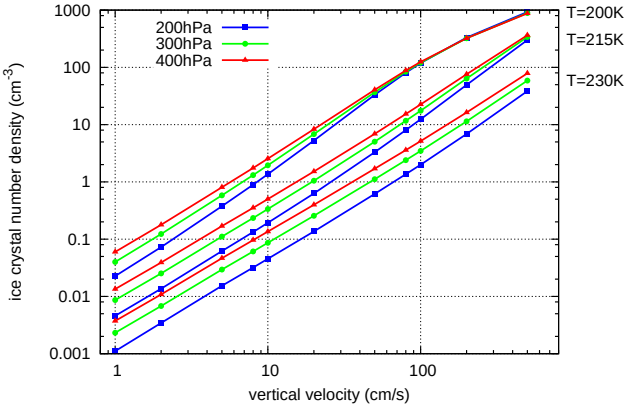

Fig. 10. Box model calculations for the homogeneously formed ice crystal number densities depending on the vertical velocity and on the temperature. For the simulations, we assume a fixed width for the aerosol size distribution of σ_r=1.4 and a geometric mean radius of r_m=25 nm. Here, the impact of pressure on the formation of ice crystals is shown using values of p=200/300/400 hPa.

In the next time step this cutoff is forgotten, however, because the bulk model always assumes the same type of size distribution. This has the effect that at each time step during nucleation (except the first) the size of freezing droplets is overestimated. The newly formed crystals come out too large, consume too much excess vapour and quench nucleation prematurely, so that eventually too few crystals are produced. We can try to mitigate this error by reducing the mean aerosol size during the nucleation phase (switched off for the idealised experiments), but this does not always help, because the error depends in a non-linear way on the time step (simply because the mass distribution is a non-linear function). Later we will see that the mentioned problems become unimportant in cases with realistic aerosol background concentrations, so that fortunately it turns out unnecessary to invent a much more complicated correction for the mean aerosol size.

With the same setup as before we now study the effect of changing the geometric mean radius of the "dry" sulphuric acid: r_m=12.5, 25.0, 50.0 nm. We hold the width constant at σ=1.4. Fig. 9 shows the results.

At the two higher temperatures there is hardly an effect of the aerosol core mass distribution. But at the lowest temperature and at high uplift rates, there is an effect. Our model follows the detailed microphysical results of Kärcher and Lohmann (2002a,b) the best when the acid mass in the droplets is smallest. In this case equilibrium between the solution droplets and their environment is easier to maintain compared to cases with larger acid fractions; hence use of the Koehler equations is still justified at strong uplift. We have already stated above that at (water) saturation the equilibrium droplet radius r_d is proportional to the square root of the solute mass, i.e. proportional to $r^{3/2}$, which shows that generally droplets are smaller with smaller solute mass under otherwise identical conditions. The relaxation time (the time needed to equilibrate with changed ambient saturation ratio) of a droplet increases with its size because the number of water molecules that have to be transferred between the vapour and the droplets increases with droplet size. A simple remedy of the problem encountered above could therefore be to choose smaller values of r_m or σ_r than in corresponding spectral microphysics simulations. As we have seen, this choice gives better results at low temperatures and high uplift velocities while it has merely a weak effect at other conditions. Such an approach is justified as long as it is rather the ice than the aerosol that is the focus of the studies.

Finally we study the pressure dependence of the number concentration of ice crystals freezing by homogeneous nucleation. We expect an influence via the pressure dependence of the diffusion coefficient. Also results of Hoyle et al. (2005) point at the possibility that changes in pressure can change the amount of ice crystals formed in a homogeneous freezing event up to one order of magnitude. We select σ_r=1.4, r_m=25 nm as a setup that gave reasonably consistent results with Kärcher and Lohmann (2002a) who, however, did not investigate the pressure dependence. We choose temperatures in the range T=200, 215, 230 K and pressures in the range p=200, 300, 400 hPa. The results are presented in Fig. 10.

We can see clearly that the ambient pressure has an impact on the ice crystal number densities produced during the cooling experiment. The diffusion constant depends on

pressure, i.e. $D_v \propto p^{-1}$ (see Eq. 31); thus diffusional growth rates decrease with increasing ambient pressure due to decreasing mean free path of the water molecules in air. Slower growth at higher pressures implies that supersaturation can stay longer above the nucleation threshold, hence more crystals nucleate. Varying the pressure from 200 to 400 hPa leads to an increase in the ice crystal number concentrations by a factor of 4–5.

4.1.2 Realistic background conditions

Realistic background aerosol concentrations are much lower than in the idealised simulations, for instance in the range $n_a = N_a \rho \sim 100-300\,\mathrm{cm}^{-3}$ (Minikin et al., 2003). Hence, we repeat the simulations of Sect. 4.1.1 with a realistic background aerosol density of $n_a = 300\,\mathrm{cm}^{-3}$. In this case we also use the correction for the mean aerosol mass, i.e. the aerosol size distribution is now shifted to smaller masses after a nucleation event. Under realistic conditions the number of ice crystals that form in homogenous nucleation events can be constrained by the available aerosol.

Figure 11 shows the impact of the width of the aerosol size distribution. We see that it hardly has an effect on the number of crystals formed, even at the lowest temperature and the highest uplift velocities (except for a very broad distribution with $\sigma_r = 1.9$). This is in sharp contrast to the idealised cases where σ_r had a much larger influence at the lowest temperature. We conclude that it is here the constraint by the available aerosol rather than the equilibrium assumptions in the Koehler and Koop theories that leads to lower crystal numbers than in the Kärcher and Lohmann (2002a) studies. This implies that the problems encountered above are less important in reality than in the idealised situations, which means that our parameterisation can be used at low temperatures and high uplift velocities.

We also repeated the simulations with different pressures with the realistic aerosol distribution. While we still find the pressure effect at low uplift speeds, the effect gets weak or even vanishes at high uplift speeds due to the constraints posed by the number of available aerosol particles (see Fig. 12).

4.1.3 Time step issues

In all previous box model simulations we have adapted the time step such that the homogeneous nucleation event can be resolved in time. However, for more expensive 2-D/3-D simulations one would like to use longer time steps. We have tested how the model behaves with fixed time steps of $\Delta t = 0.1, 0.5, 1.0, 2.0\,\mathrm{s}$, respectively, both in the idealised and realistic cases from above. Figure 13 shows the results.

Obviously, problems appear with too long time steps at high uplift speeds. While there are no problems even with a time step of 1 s at small vertical velocities ($w \leq 20-50\,\mathrm{cm\,s}^{-1}$), there are strong deviations from the previously shown cases at higher vertical velocities ($w > 50\,\mathrm{cm\,s}^{-1}$) where the non-linear behaviour of both, the

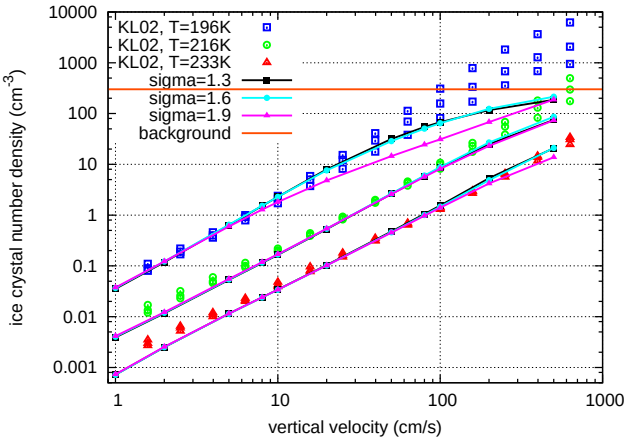

Fig. 11. Box model calculations for the homogeneously formed ice crystal number densities depending on the vertical velocity and on the temperature. For comparisons, the values from detailed microphysics calculations in Kärcher and Lohmann (2002a) are shown. For the simulations, we assume a fixed geometric mean size of the aerosol distribution ($r_m = 25.0\,\mathrm{nm}$). Here, the impact of different width of the aerosol distribution is shown (black: $\sigma_r = 1.3$, cyan: $\sigma_r = 1.6$, magenta: $\sigma_r = 1.9$). In contrast to the simulations shown in Fig. 7, we use realistic background concentrations for the sulphuric acid aerosol ($n_c = 300\mathrm{cm}^{-3}$). This leads to less ice crystals for low temperatures and/or high vertical velocities due to a limited reservoir of solution droplets.

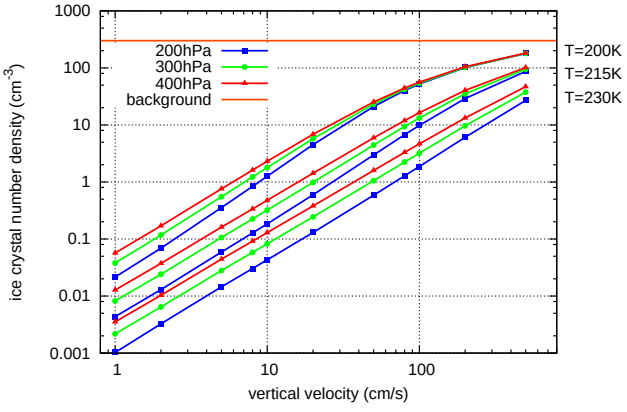

Fig. 12. Box model calculations for the homogeneously formed ice crystal number densities depending on the vertical velocity and on the temperature. For the simulations, we assume a fixed width for the aerosol size distribution of $\sigma_r = 1.4$ and a geometric mean radius of $r_m = 25\,\mathrm{nm}$. Here, the impact of pressure on the formation of ice crystals is shown using values of $p = 200/300/400\,\mathrm{hPa}$. In contrast to the simulations showed in Fig. 10, we use realistic background concentrations for the sulphuric acid aerosol ($n_c = 300\mathrm{cm}^{-3}$). This leads to less ice crystals for low temperatures and/or high vertical velocities due to a limited reservoir of solution droplets.

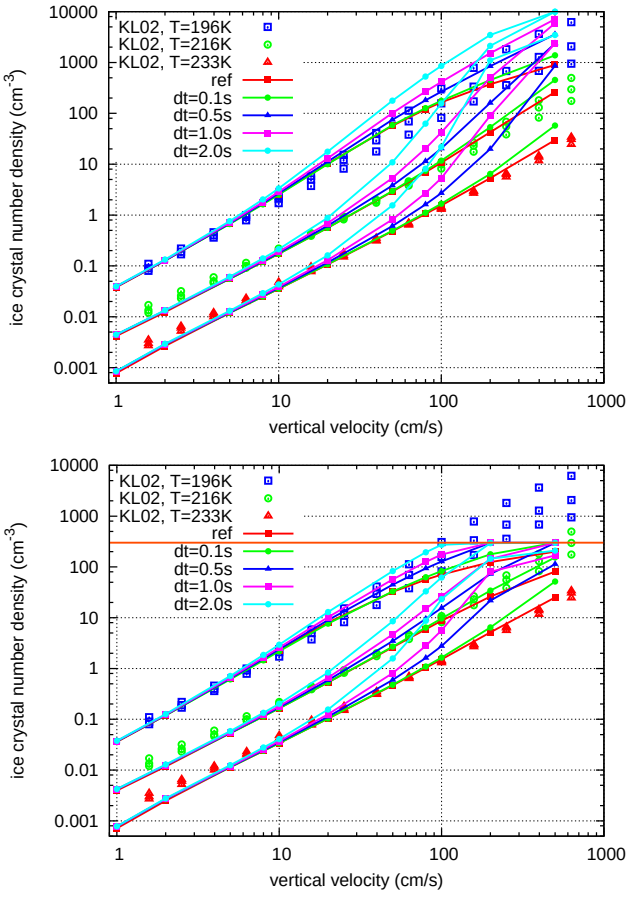

Fig. 13. Box model calculations for the homogeneously formed ice crystal number densities depending on the vertical velocity and on the temperature. For comparison, the values from detailed microphysics calculations in Kärcher and Lohmann (2002a) are shown. For the simulations, we assume a fixed width for the aerosol distribution of σ_r=1.4 and a geometric mean radius of r_m=25 nm. Here, the impact of the prescribed (fixed) time step (dt=0.1/0.5/1.0/2.0) for the simulations is shown, compared to simulations using an adapted time step (simulation "ref", red line). For the simulations shown at the top panel, the background aerosol reservoir is large, while for the simulations at the bottom panel, we used a realistic background aerosol concentration (n_c=300cm^{-3}).

nucleation process and the depositional growth introduce large deviations from the reference cases. The deviations are more severe for higher than colder temperatures. Crystal growth proceeds faster at warmer than at colder temperatures, which means that the duration of the nucleation pulse increases with decreasing temperature. When the nucleation event is not resolved, its duration will be overestimated and too much crystals will form. This effect is evidently the more severe the shorter is the nucleation pulse; i.e. the largest error occurs at the warmest temperature considered.

4.2 Formation and evolution of an arctic cirrostratus

In this section we compare the performance of our bulk microphysics scheme with the spectrally resolving schemes of Lin et al. (2005) and Kärcher (2005) for the case of an arctic cirrostratus triggered by a constant vertical updraught.

4.2.1 Setup

We use the following setup for our simulations: The whole 2D model domain ($0 \le x \le 6.3$ km, $2 \le z \le 11$ km) is lifted up adiabatically with a constant updraught velocity of w=0.05 m s^{-1} as described in Kärcher (2005). This is equivalent to a constant cooling of the background profile T_e with a rate of $dT/dt = dT/dz \cdot dz/dt = -g/c_p \cdot w = -0.000489$ K/s. The same cooling rate was used in the box model simulations in Sect. 4.1. The cooling is adiabatic (i.e. θ_e is constant), and is continued for a total simulation time of t_s=7 h. In Fig. 14 the initial profiles for the simulations are shown.

We use a horizontal resolution of Δx=100 m with a horizontal extension of 6.3 km, cyclic boundary conditions in x-direction, a vertical resolution of Δz=10 m and a dynamical time step of Δt=1 s. According to our discussion in Sect. 4.1.3, there is no need of a small microphysical time step for the moderate vertical updraught in this case. For the background aerosol (H_2SO_4) we use a number density of $n_a = N_a \rho$=300 cm^{-3} with geometric standard deviation σ_r=1.4 and geometric mean radius of r_m=25 nm for the lognormal distribution, as these values gave good results in Sect. 4.1.

4.2.2 Results

For our comparisons we mostly refer to the simulation by Kärcher (2005), because he also parameterised homogeneous nucleation according to Koop et al. (2000).

In Fig. 15 the time evolution of the variables relative humidity wrt ice, ice crystal mass and number concentrations, resp., are shown.

The first nucleation event occurs at $t \approx 60$ min. The supersaturation peak of about 154% RHi triggers homogeneous nucleation. Within a few minutes a large amount of ice crystals ($N_c \rho \sim 100$ L^{-1}) is formed. Because of the high supersaturation the ice crystals can grow quickly and deplete a fraction of the water vapour, which reduces the relative humidity, see Fig. 16. Ice crystals grow and soon start to fall. Therefore the peak of high supersaturation at the top of the ISSR is influenced very weakly by the depletion of the water vapour. The peak is permanently maintained for the whole simulation time and is a permanent source for homogeneous nucleation at the top of the ISSR.

The combination of crystal growth and sedimentation causes two effects: On the one hand, the supersaturation is reduced by crystal growth such that the relative humidity cannot reach the threshold for homogeneous nucleation in

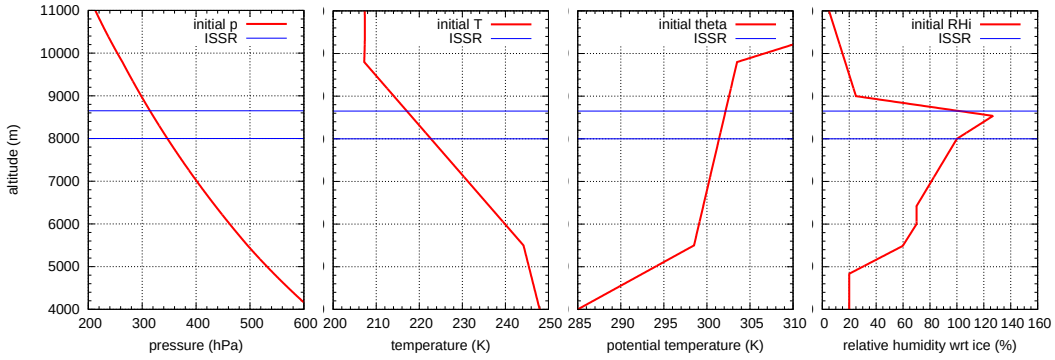

Fig. 14. Initial vertical profiles (pressure, temperature, potential temperature and relative humidity wrt ice) for the simulations of a synoptically driven cirrostratus.

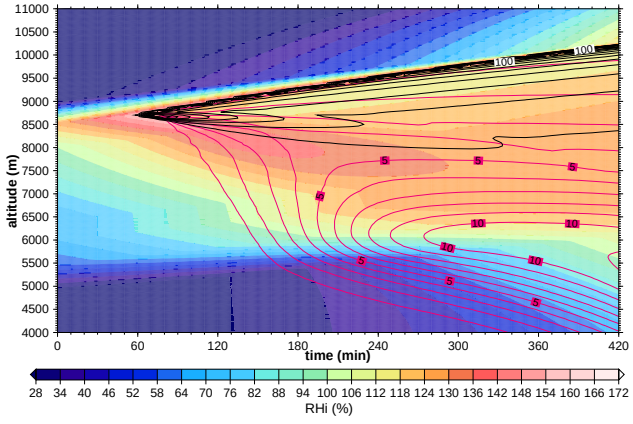

Fig. 15. Time evolution of the simulated cirrostratus lifted with a constant vertical velocity of w=0.05 m s^{-1}. The colours indicate relative humidity wrt ice, while lines indicate ice crystal number densities (black, in L^{-1}, Δn_c=10L^{-1}) and ice water content (purple, in mg m^{-3}, ΔIWC = 1mg m^{-3}).

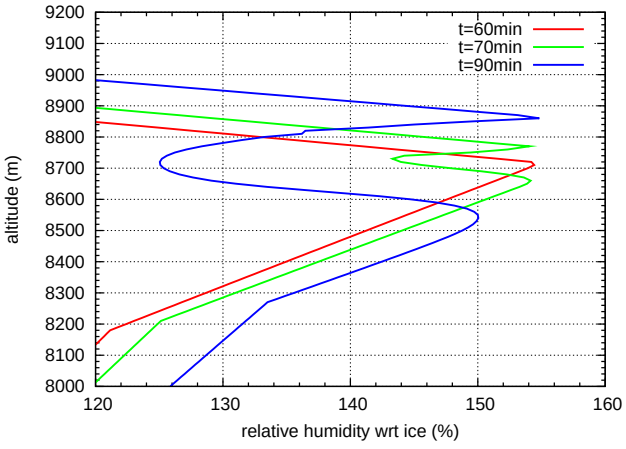

Fig. 16. Temporal evolution of the vertical RHi profiles for simulation time 60≤t≤90 min. The notch of the profile due to ice crystal growth is represented clearly, while the supersaturation at the cloud top remains.

the lower part of the cloud. On the other hand, the falling ice crystals formed at the top of the cloud are the only sink for the water vapour. Although the continuous homogeneous nucleation events permanently form new ice crystals, these are spread vertically over the whole cloud depth resulting in relatively low number densities. Thus, inside the cloud, ice supersaturation is maintained. If there were no sedimentation or if it were very weak, the cooling in the supersaturated layer would everywhere lead to nucleation, then the crystals would grow until the excess vapour would be consumed over the whole depth of the layer. Sedimentation obviously plays a crucial role for the development and the structure of the simulated cirrus cloud and for the maintenance of supersaturation within the cloud.

The first nucleation event forms a large number of ice crystals. Many crystals fall downwards, resulting in a downward moving peak of high ice crystal number densities in Fig. 17.

These results agree qualitatively well with those of Kärcher (2005), yet there are differences in details. For instance, the in-cloud supersaturation is higher in our simulation than in Kärcher's. This is simply a consequence of different assumptions of crystal shape in the two codes. While we use hexagonal columns with an aspect ratio r_a>1 for crystal lengths L≥7.42 μm, Kärcher (2005) assumes spherical crystals (r_a=1) for crystal lengths up to L∼25 μm; spherical crystals always grow faster than columns. Hence high supersaturation can be maintained for a longer period in our simulation than in Kärcher's. Second, our treatment of sedimentation is more diffusive than that of Kärcher (2005) who uses a particle approach with the advection scheme by Walcek (2000). Numerical diffusion in the double-moment scheme (see Wacker and Seifert, 2001) leads to smoothing of vertical gradients in ice crystal number concentrations and cloud ice mixing ratio, such that peak values are smaller than in Kärcher (2005).

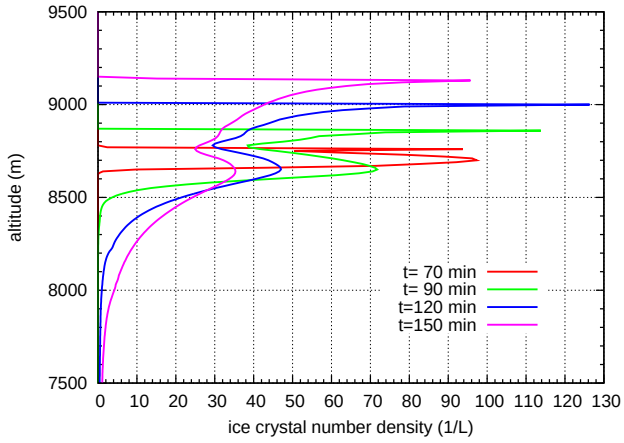

Fig. 17. Downward moving peak of high ice crystal number densities formed by the first homogeneous nucleation event at $t \approx 60$ min in the reference simulation (i.e. constant uplift of $w = 0.05\,\mathrm{m\,s^{-1}}$). At the top of the cloud there is continuous nucleation, indicated by the high peak values of ice crystal number density.

In spite of these differences in details we find that our bulk microphysics scheme is able to well reproduce the main features of the arctic cirrostratus case, namely:

- High supersaturation at the top of the cloud with continuously ongoing homogeneous nucleation;
- Significant supersaturation within the cloud for the whole simulation time;
- Downward moving peak of high ice crystal number concentrations formed at the first nucleation event.

Lin et al. (2005) noted that high vertical resolution is needed for the reproduction of these features. We have checked this issue using various resolutions in the range $5 \leq z \leq 50$ m. It turned out that the number of ice crystals that are produced is underestimated with too coarse vertical resolution, which occurs when the continuous nucleation source at the cloud top is unresolved. This renders the supersaturation inside the cloud too high. Results change only marginally between simulations with resolutions of $\Delta z = 5$ m and $\Delta z = 10$ m. Therefore, we used $\Delta z = 10$ m.

Regarding the occurrence of ice supersaturation inside cirrus clouds we want to remark that this feature is not limited to the very cold temperature range in the tropics (an example is presented by Gao et al., 2004). Also in the temperature range of midlatitude and arctic cirrus clouds ice supersaturation inside the clouds can be found frequently, see for instance the results of Ovarlez et al. (2002); Comstock et al. (2004); Krämer et al. (2008) and also the recent SPARC newsletter about the supersaturation issue (Peter et al., 2008).

5 Conclusions

We have described a new bulk microphysics parameterisation for simulation of cirrus clouds on the cloud resolving scale. In the two-moment scheme the processes nucleation (homogeneous and heterogeneous), deposition growth/sublimation and sedimentation of ice crystals are implemented. An arbitrary number of ice classes can be treated that are discriminated by their formation mechanism. Each ice class is connected to an aerosol type that freezes into the respective ice class. We tried to formulate process rates as functions of general moments of the assumed underlying ice mass distribution in order to keep the model flexible enough that various kinds of mass distribution can be chosen. Currently we use log-normal distributions for the aerosol and the ice masses. The new parameterisation was implemented into a simple box model and into the anelastic, non-hydrostatic model EULAG.

In a first validation step we compared the ice crystal number densities generated during box model simulations with a steady and constant updraught with results from a box model that was equipped with a more detailed microphysics scheme (Kärcher and Lohmann, 2002a). The agreement of our results with the results from the detailed model was very good. Additionally we used the box model to study the impact of the ambient pressure on the generated ice crystal number concentrations. Also, for realistic background aerosol conditions simulations were carried out. In this case we could find that the background aerosol acts as a limiting factor, i.e. the produced ice crystal number density is strongly reduced in the low temperature range in combination with high vertical velocities (consistent with results of Kay and Wood, 2008). This partly offsets the underestimation of ice crystal number densities of our parameterisation. Additionally, the pressure dependence of the parameterisation was investigated.

In a second validation step we simulated the case of an arctic cirrostratus using EULAG as a 1-D column model first. Also in this case the agreement with a much more detailed microphysical model (Kärcher, 2005) was very good.

These studies led to the following conclusions:

- The model is validated against models with detailed microphysics and produces reliable results;
- Sedimentation is of utmost importance in the evolution of the cloud structure and the in-cloud humidity field;
- Persistent in-cloud supersaturation is found in our simulations consistent with Kärcher (2005).

Finally, we conclude that the model is suitable to represent cirrus clouds in cloud-resolving simulations. In the second part of our study (Spichtinger and Gierens, 2009), we will investigate the validation case of an arctic cirrostratus carefully in terms of changing the large scale dynamics (i.e. updraught velocity) and in terms of possible changes due to 2-D effects

introduced by temperature fluctuations and wind shear. In future applications the model will be used for investigating the effects of the competition of different nucleation mechanisms (Spichtinger and Gierens, 2008) and for the multi-scale problem of the impact of mesoscale dynamics on the formation and evolution of cirrus clouds (as in Spichtinger and Dörnbrack, 2006).

Appendix A: Notation

a	long half axis of spheroid
$a(p,T)$	factor for Koenig's approximation (abbrev. by a)
a_w	water activity in the solution
a_w^i	water activity in the solution in equilib. with ice
A	Ice crystal surface
A'	$=\sqrt{a^2-b^2}$
b	short half axis of spheroid
$b(p,T)$	exponent for Koenig's approximation (abbrev. by b)
C	Capacitance factor
c_p	heat capacity for constant pressure
$c(T,p)$	correction factor for sedimentation
$\frac{D}{Dt}$	advection operator/total derivative
D	ice crystal diameter
D_v	Diffusion constant
e	water vapour pressure
e_i^*	saturation water vapour pressure over ice
e_w^*	saturation water vapour pressure over water
F_θ	additional forcing for potential temperature
$\mathbf{f}$	Coriolis vector
$f(m)$	ice crystal mass distribution
f_1	correction, kinetic growth regime (mass growth rate)
f_2	correction, ventilation (mass growth rate)
f_1^*	correction, kinetic growth regime (latent heat release)
f_2^*	correction, ventilation (latent heat release)
$f_a(m)$	aerosol mass distribution
$f_a'(m)$	aerosol mass distribution, normalised to 1
f_m	mass concentration fraction (aerosol)
f_n	number concentration fraction (aerosol)
f_N	number concentration fraction (ice)
f_q	mass concentration fraction (ice)
$\mathbf{g}$	gravity vector
g	gravitational acceleration
L	ice crystal length
L_i	$i=1,2,3$ transition sizes for terminal velocity
L_m	geometric mean size in lognormal distribution
l_m^*	reference length for kinetic correction (mass)
l_Q^*	reference length for kinetic correction (heat)
L_s	latent heat of sublimation
L_t	transition size between spherical crystals and columns
$\mathbf{M}$	metric term
m	(ice crystal) mass
$\overline{m}$	mean mass
$m_0(p,T)$	mass for appr. in Eq. (38) (abbrev. m_0)
m_i	i=1, 2, 3 transition masses for terminal velocity
m_m	geometric mean mass in lognormal distribution
m_{pre}	predominant mass
m_t	transition mass between spherical crystals and columns
M_w	molecular weight of water vapour
N_a	aerosol number concentration per kg dry air
n_a	aerosol number density (n_a=$N_a\rho$) per m^3 dry air
N_c	ice crystal number concentration per kg dry air
n_c	ice crystal number density (n_c=$N_c\rho$) per m^3 dry air
N_{Pr}	Prandtl number
N_{Re}	Reynolds number
N_{Sc}	Schmidt number
P	freezing probability
p	pressure
p'	pressure deviation
p_0	reference pressure = 101 325 hPa
$p_{0,1}$	reference pressure = 30 000 hPa
$p_{0,2}$	reference pressure = 81 500 hPa
p_e	pressure, environmental state
q_a	aerosol mass mixing ratio
q_c	cloud ice mass mixing ratio
q_v	specific humidity
q_{ve}	specific humidity, environmental state
r	radius
r^*	effective crystal radius for growth
r_0	ratio of predominant and mean mass
r_a	aspect ratio
r_d	radius of solution droplets
r_m	geometric mean radius in lognormal distribution
R	universal gas constant
R_g	ideal gas constant for dry air
R_v	ideal gas constant for water vapour
RH	relative humidity with respect to water
RHi	relative humidity with respect to ice
t	time
t_s	simulation time
T	temperature
T_e	temperature, environmental state
T_0	reference temperature =273.15 K
$T_{0,1}$	reference temperature =233 K
$T_{0,2}$	reference temperature =270 K
T_S	temperature at ice surface
$\mathbf{u}$	velocity field
$\mathbf{u}'$	velocity field deviation
$\mathbf{u}_e$	velocity field, environmental state
u	horizontal wind
$\overline{u_r}$	average thermal velocity of air molecules
V_d	solution droplet volume
$v(m)$	terminal velocity of a single ice crystal
$v_0(m)$	reference terminal velocity of a single ice crystal
v_m	mass weighted terminal velocity
v_n	number weighted terminal velocity
w	vertical velocity
w_w	H_2O weight fraction
x	horizontal coordinate

x	coefficient for terminal velocity
y	coefficient for terminal velocity
z	vertical coordinate
α	exponent for mass/number fraction (Eq. 29)
α_d	deposition coefficient
β_d	thermal accommodation coefficient
$\gamma(p,T)$	exponent for appr. in Eq. (38) (abbrev. γ)
$\gamma(m)$	factor for terminal velocity
δ	coefficient for approximation in (Eq. 38)
$\delta(m)$	exponent for terminal velocity
ϵ'	eccentricity of an ellipse
ϵ	ratio of gas constants for dry air and water vapour
ϵ_p	$=(1/\epsilon)-1$
μ_k	kth moment of probability distribution f
ρ	air density
$\bar{\rho}$	air density, base state
ρ_b	bulk ice density
ρ_d	solution density
$\rho_{s,i}$	saturated water vapour density at crystal surface
ρ_v	water vapour partial density
σ_L	geometric std. dev., size distribution (ice)
σ_m	geometric std. dev., mass distribution (ice)
σ_r	geometric std. dev., radius distribution (aerosol)
θ	potential temperature
θ'	potential temperature deviation
θ_d	density potential temperature, (Eq. 4)
θ'_d	density potential temperature deviation
θ_{de}	density potential temperature, environmental state
θ_e	potential temperature, environmental state
$\bar{\theta}$	potential temperature, base state

Acknowledgements. We are grateful to Piotr K. Smolarkiewicz for sharing his model and Andreas Dörnbrack for help in using the model. Both of these and Marcia Baker, Bernd Kärcher, Ulrike Lohmann, Thomas Peter, Olaf Stetzer and Marian deReus stimulated the work with many fruitful discussions. This study contributes to the DFG (German research foundation) project "Dünner Zirrus" (GI 333/1-1) and to the DLR/HGF-project "Particles and Cirrus Clouds" (PAZI-2). The numerical simulations were carried out at the European Centre for Medium-Range Weather Forecasts (special project "Ice supersaturation and cirrus clouds").

Edited by: P. Haynes

References

Barthazy, E. and Schefold, R.: Fall velocity of snowflakes of different riming degree and crystal types, Atmos. Res., 82, 391–398, 2006.

Bailey, M. and J. Hallet, 2004: Growth rates and habits of ice crystals between –20 and –70°C, J. Atmos. Sci., 61, 514–544.

Bunz, H., Benz, S., Gensch, I., and Krämer, M.: MAID: a model to simulate UT/LS aerosols and ice clouds, Environ. Res. Lett., 3, 035001, doi: 10.1088/1748-9326/3/3/035001, 2008.

Chen, T., Rossow, W. B., and Zhang, Y.: Radiative Effects of Cloud-Type Variations, J. Climate, 13, 264–286, 2000.

Chiruta, M. and Wang, P. K.: The capacitance of solid and hollow hexagonal ice columns, Geophys. Res. Lett., 32, L05803, doi:10.1029/2004GL021771, 2005.

Comstock, J., Ackerman, T. P., Turner, D. D.: Evidence of high ice supersaturation in cirrus clouds using ARM Raman lidar measurements, Geophys. Res. Lett., 31, L11106, doi:10.1029/2004GL019705, 2004.

Emanuel, K.: Atmospheric convection. Oxford University Press, 580 pp., 1994.

Fusina, F., Spichtinger, P., and Lohmann, U.: The impact of ice supersaturated regions and thin cirrus on radiation in the mid latitudes, J. Geophys. Res., 112, D24S14, doi:10.1029/2007JD008449, 2007.

Gao, R. S., Popp, P.J., Fahey, D.W., et al.: Evidence that nitric acid increases relative humidity in low-temperature cirrus clouds, Science, 303, 516–520, 2004.

Gayet, J.-F., Shcherbakov, V., Mannstein, H., Minikin, A., Schumann, U., Ström, J., Petzold, A., Ovarlez, J., and Immler, F.: Microphysical and optical properties of midlatitude cirrus clouds observed in the southern hemisphere during INCA, Q. J. Roy. Meteror. Soc., 132, 2719–2748, 2006.

Gettelman, A., Fetzer, E. J., Eldering, A., Irion, F. W.: The global distribution of supersaturation in the upper troposphere from the atmospheric infrared sounder, J. Climate, 19, 6089–6103, 2006.

Gierens, K.: Numerical simulations of persistent contrails, J. Atmos. Sci., 53, 3333–3348, 1996.

Gierens, K. M. and Ström, J.: A numerical study of aircraft wake induced ice cloud formation, J. Atmos. Sci. 55, 3253–3263, 1998.

Gierens, K., Schumann, U., Helten, M., Smit, H., and Marenco, A.: A distribution law for relative humidity in the upper troposphere and lower stratosphere derived from three years of MOZAIC measurements, Ann. Geophys., 17, 1218–1226, 1999, http://www.ann-geophys.net/17/1218/1999/.

Gierens, K.: On the transition between heterogeneous and homogeneous freezing, Atmos. Chem. Phys., 3, 437–446, 2003, http://www.atmos-chem-phys.net/3/437/2003/.

Gierens, K., Monier, M., and Gayet, J.-F.: The deposition coefficient and its role for cirrus clouds, J. Geophys. Res., 108, 4069, doi:10.1029/2001JD001558, 2003.

Grabowski, W. and Smolarkiewicz, P.: A multiscale anelastic model for meteorological research, Mon. Weather Rev., 130, 939–956, 2002.

Haag, W., Kärcher, B., Schurath, U., Möhler, O., Stetzer, O., Schaefers, S., Schiller, C., and Krämer, M.: Numerical simulations of homogeneous freezing processes in the aerosol chamber AIDA, Atmos. Chem. Phys., 3, 195–210, 2003a, http://www.atmos-chem-phys.net/3/195/2003/.

Haag, W. and Kärcher, B., Ström, J., Minikin, A., Lohmann, U., Ovarlez, J., and Stohl, A.: Freezing thresholds and cirrus cloud formation mechanisms inferred from in situ measurements of relative humidity, Atmos. Chem. Phys., 3, 1791–1806, 2003b, http://www.atmos-chem-phys.net/3/1791/2003/.

Haag, W. and Kärcher, B.: The impact of aerosols and gravity waves on cirrus clouds at midlatitudes, J. Geophys. Res., 109, D12202, doi:10.1029/2004JD00457, 2004.

Hall, W. D. and Pruppacher, H. R.: The survival of ice particles falling from cirrus clouds in subsaturated air, J. Atmos. Sci., 33,

1995–2006, 1976.

Harrington, J. Y., Meyers, M. P., Walko, R. L., and Cotton, W. R.: Parameterization of ice crystal conversion processes due to vapor deposition for mesoscale models using double-moment basis functions. Part I: Basic formulation and parcel model test, J. Atmos. Sci., 52, 4344–4366, 1995.

Heymsfield, A. J. and Sabin, R. M.: Cirrus crystal nucleation by homogeneous freezing of solution droplets, J. Atmos. Sci., 46, 2252–2264, 1989.

Heymsfield, A. and Iaquinta, J.: Cirrus crystal terminal velocities, J. Atmos. Sci., 57, 916–938, 2000.

Heymsfield, A. and McFarquhar, G. M.: Mid-latitude and tropical cirrus: Microphysical properties. In: *Cirrus* [D.K. Lynch, K. Sassen, D. O'C. Starr, G. Stephens (Eds.)]. Oxford University Press, Oxford, U.K., 78–101, 2002

Höller, H.: Parameterization of cloud-microphysical processes in a three-dimensional convective mesoscale model, Forschungsbericht, Deutsche Forschungs- und Versuchsanstalt für Luft- und Raumfahrt, DFVLR FB 86-02, 82 pp., ISSN 0171-1342, 1986.

Hoyle, C., Luo, B., and Peter, T.: The origin of high ice crystal number densities in cirrus clouds, J. Atmos. Sci., 62, 2568–2579, 2005.

IPCC: Climate Change 2007: The Physical Science Basis. in: Contribution of Working Group I to the Fourth Assessment Report of the Intergovernmental Panel on Climate Change, edited by: Solomon, S., Qin, D., Manning, M., Chen, Z.,Marquis, M., Averyt, K. B., Tignor, M., and Miller, H. L., Cambridge University Press, Cambridge, United Kingdom and New York, NY, USA, 996 pp., 2007.

Jawitz, J. W.: Moments of truncated continuous univariate distributions, Adv. Water Res., 27, 269–281, 2004.

Jensen, E. J., Toon, O. B., Westphal, D. L., Kinne, S., and Heymsfield, A. J.: Microphysical modeling of cirrus 1. Comparison with 1986 FIRE IFO measurements, J. Geophys. Res., 99(D5), 10421–10442, doi:10.1029/93JD02334, 1994.

Kajikawa, M. and Heymsfield, A.: Aggregation of ice crystals, J. Atmos. Sci., 46, 3108–3121, 1989.

Kärcher, B.: Supersaturation, dehydration, and denitrification in Arctic cirrus, Atmos. Chem. Phys., 5, 1757–1772, 2005, http://www.atmos-chem-phys.net/5/1757/2005/.

Kärcher, B. and Lohmann, U.: A Parameterization of cirrus cloud formation: Homogeneous freezing of supercooled aerosols, J. Geophys. Res., 107(D2), 4010, doi:10.1029/2001JD000470, 2002a.

Kärcher, B. and Lohmann, U.: A parameterization of cirrus cloud formation: Homogeneous freezing including effects of aerosol size, J. Geophys. Res., 107, D23, D01205, doi:10.1029/2001JD001429, 2002b.

Kärcher, B., Hendricks, J., and Lohmann, U.: Physically-based parameterization of cirrus cloud formation for use in global atmospheric models, J. Geophys. Res., 111, D01205, doi:10.1029/2005JD006219, 2006.

Kay, J. and Wood, R.: Timescale analysis of aerosol sensitivity during homogeneous freezing and implications for upper tropospheric water vapor budgets, Geophys. Res. Lett., 35, L10809, doi:10.1029/2007GL032628, 2008.

Kessler, E.: On the distribution and continuity of water substance in atmospheric circulations, Meteor. Monogr., 32, Am. Meteorol. Soc., 84 pp., Boston, 1969.

Koenig, L.: Numerical modeling of ice deposition, J. Atmos. Sci., 28, 226–237, 1971.

Koop, T., Luo, B., Tsias, A., and Peter, T.: Water activity as the determinant for homogeneous ice nucleation in aqueous solutions, Nature 406, 611–614, 2000.

Krämer, M., Schiller, C., Afchine, A., Bauer, R., Gensch, I., Mangold, A., Schlicht, S., Spelten, N., Sitnikov, N., Borrmann, S., de Reus, M., Spichtinger, P.: Ice supersaturations and cirrus cloud crystal numbers, Atmos. Chem. Phys. Discuss., 8, 21089–21128, 2008, http://www.atmos-chem-phys-discuss.net/8/21089/2008/.

Lee, S.-H., Wilson, J. C. Baumgardner, D., Herman, R. L., Weinstock, E. M., LaFleur, B. G., Kok, G., Anderson, B., Lawson, P., Baker, B., Strawa, A., Pittman, J. V., Reeves, J. M., and Bui, T. P.: New particle formation observed in the tropical/subtropical cirrus clouds, J. Geophys. Res., 109, D20209, doi:10.1029/2004JD005033, 2004.

Libbrecht, K. G.: The physics of snow crystals, Rep. Prog. Phys., 68, 855–895, 2005.

Lin, R.-F., Starr, D., DeMott, P., Cotton, R., Sassen, K., Jensen, E., Kärcher, B., and Liu, X.: Cirrus Parcel Model Comparison Project. Phase 1: The critical components to simulate cirrus initiation explicitly, J. Atmos. Sci., 59, 2305–2329, 2002.

Lin, R.-F., Starr, D., Reichardt, J., and DeMott, P.: Nucleation in synoptically forced cirrostratus, J. Geophys. Res., 110, D08208, doi:10.1029/2004JD005362, 2005.

Liu, X., Penner, J. E., Ghan, S. J., and Wang, M.: Inclusion of Ice Microphysics in the NCAR Community Atmospheric Model Version 3 (CAM3), J. Climate, 20, 4526–4547, 2007.

Lohmann, U. and Kärcher, B.: First interactive simulations of cirrus clouds formed by homogeneous freezing in the ECHAM GCM, J. Geophys. Res., 107, 4105, doi:10.1029/2001JD000767, 2002.

Magee, N., Moyle, A. M., Lamb, D.: Experimental determination of the deposition coefficient of small cirrus-like ice crystals near -50°C, Geophys. Res. Lett., 33, L17813, doi:10.1029/2006GL026665, 2006.

McDonald, J. E.: Use of the electrostatic analogy in studies of ice crystal growth, ZAMP, 14, 610–620, 1963

Meyers, M. P., DeMott, P. J., and Cotton, W. R.: New primary ice-nucleation parameterizations in an explicit cloud model, J. Appl. Meteorol., 31, 708–721, 1992.

Minikin, A., Petzold, A., Ström, J., Krejci, R., Seifert, M., van Velthoven, P., Schlager, H., and Schumann, U.: Aircraft observations of the upper tropospheric fine particle aerosol in the Northern and Southern Hemispheres at midlatitudes, Geophys. Res. Lett., 30, 1503, doi:10.1029/2002GL016458, 2003.

Murphy, D. and Koop, T.: Review of the vapour pressure of ice and supercooled water for atmospheric applications, Q. J. Roy. Meteror. Soc., 131, 1539–1565, 2005.

Ovarlez, J., Gayet, J.-F., Gierens, K., Ström, J., Ovarlez, H., Auriol, F., Busen, R.,Schumann,U.: Water vapor measurements inside cirrus clouds in northern and southern hemispheres during INCA, Geophys. Res. Lett., doi:10.1029/2001GL014440, 2002.

Peter, T., Marcolli, C., Spichtinger, P., Corti, T., Baker M. B., and Koop, T.: When dry air is too humid, Science, 314 (5804), 1399–1400, 2006.

Peter, T., Kraemer, M., and Moehler, O.: Upper Tropospheric Humidity, SPARC/WCRP Newsletter 30, 9–15, 2008.

Phillips, V. T. J., Choularton, T. W., Illingworth, A. J., Hogan, R. J.,

and Field, P. R. Simulations of the glaciation of a frontal mixed-phase cloud with the Explicit Microphysics Model, Q. J. Roy. Meteror. Soc., 129, 1351–1371, 2003.

Pruppacher, H. and Klett, J.: Microphysics of Clouds and Precipitation, Kluwer Acad. Pub., Dordrecht, 954 pp., 1997

Reisner, J., Rasmussen, R. M., and Bruintjes, R. T.: Explicit forecasting of supercooled liquid water in winter storms using the MM5 mesoscale model, Q. J. Roy. Meteror. Soc., 124, 1071–1107, 1998.

Sassen, K. and Dodd, G. C.: Homogeneous nucleation rate for highly supercooled cirrus cloud droplets, J. Atmos. Sci., 45, 1357–1369, 1988.

Sassen, K. and Dodd, G. C.: Haze particle nucleation simulations in cirrus clouds, and applications for numerical and lidar studies, J. Atmos. Sci., 46, 3005–3014, 1989.

Schröder, F., Kärcher, B., Duroure, C., Ström, J., Petzold, A., Gayet, J.-F., Strauss, B., Wendling, P., and Borrmann, S.: On the transition of contrails into cirrus clouds, J. Atmos. Sci., 57, 464–480, 2000.

Seifert, A. and Beheng, K. D.: A two-moment cloud microphysics parameterization for mixed-phase clouds. Part 1: Model description, Meteorol. Atmos. Phys., 92, 45–66, 2005.

Smolarkiewicz, P. and Margolin,L.: On forward-in-time differencing for fluids: an Eulerian/Semi-Lagrangian non-hydrostatic model for stratified flows, Atmos.-Ocean., 35, 127–152, 1997.

Smolarkiewicz, P. K. and Margolin, L. G.: MPDATA: A positive definite solver for geophysical flows, J. Comput. Phys., 140, 459–480, 1998.

Smolarkiewicz, P., Margolin, L., and Wyszogrodzki, A.: A class of nonhydrostatic global models, J. Atmos. Sci., 58, 349–364, 2001.

Spichtinger, P., Gierens, K., Leiterer, U., and Dier, H.: Ice supersaturation in the tropopause region over Lindenberg, Germany, Meteorol. Z., 12, 143–156, 2003a.

Spichtinger, P., Gierens, K., and Read, W.: The global distribution of ice supersaturated regions as seen by the microwave limb sounder, Q. J. Roy. Meteror. Soc., 129, 3391–3410, 2003b.

Spichtinger, P., Gierens, K., Smit, H. G. J., Ovarlez, J., and Gayet, J.-F.: On the distribution of relative humidity in cirrus clouds. Atmos. Chem. Phys., 4, 639–647, 2004, http://www.atmos-chem-phys.net/4/639/2004/.

Spichtinger, P., Gierens, K., and Wernli, H.: A case study on the formation and evolution of ice supersaturation in the vicinity of a warm conveyor belt's outflow region, Atmos. Chem. Phys., 5, 973–987, 2005a, http://www.atmos-chem-phys.net/5/973/2005/.

Spichtinger, P., Gierens, K., and Dörnbrack, A.: Formation of ice supersaturation by mesoscale gravity waves, Atmos. Chem. Phys., 5, 1243–1255, 2005b, http://www.atmos-chem-phys.net/5/1243/2005/.

Spichtinger P. and Dörnbrack, A.: Microphysical modeling of orographic cirrus clouds, Proceedings of the 12th AMS Conference on Cloud Physics, Madison, USA, 2006.

Spichtinger, P. and Gierens, K.: Modelling of cirrus clouds – Part 1b: Structuring cirrus clouds by dynamics, Atmos. Chem. Phys., 9, 707–719, 2009, http://www.atmos-chem-phys.net/9/707/2009/.

Spichtinger, P. and Gierens, K. M.: Modelling of cirrus clouds – Part 2: Competition of different nucleation mechanisms, Atmos. Chem. Phys. Discuss., 8, 9061–9098, 2008, http://www.atmos-chem-phys-discuss.net/8/9061/2008/.

Starr, D. and Cox, S.: Cirrus clouds. Part I: A Cirrus Cloud Model, J. Atmos. Sci., 42, 2663–2681, 1985.

Stephens, G.: The influence of radiative transfer on the mass and heat budgets of ice crystals falling in the atmosphere, J. Atmos. Sci., 40, 1729–1739, 1983.

Tompkins, A., Gierens, K., and Rädel, G.: Ice supersaturation in the ECMWF integrated forecast system, Q. J. Roy. Meteror. Soc., 133, 53–63, 2007.

Wernli, H. and Davies, H.: A Lagrangian-based analysis of extratropical cyclones. I: The method and some applications, Q. J. Roy. Meteror. Soc., 123, 467–489, 1997.

Walcek, C.: Minor flux adjustment near mixing ratio extremes for a simplified yet highly accurate monotonic calculation of tracer advection, J. Geophys. Res., 105, 9335–9348, 2000.

Wacker, U. and Seifert, A.: Evolution of rain water profiles resulting from pure sedimentation: Spectral vs. parameterized description, Atmos. Res., 58, 19–39, 2001.

Wendisch, M., Pilewskie, P., Pommier, J., Howard, S., Yang, P., Heymsfield, A. J., Schmitt, C. G., Baumgardner, D., and Mayer, B.: Impact of cirrus crystal shape on solar spectral irradiance: A case study for subtropical cirrus, J. Geophys. Res., 110, D03202, doi:10.1029/2004JD005294, 2005.

Wendisch, M., Yang, P., and Pilewskie, P.: Effects of ice crystal habit on thermal infrared radiative properties and forcing of cirrus, J. Geophys. Res., 112, D08201, doi:10.1029/2006JD007899, 2007.

Wood, S. E., Baker, M. B., and Calhoun, D.: New model for the vapor growth of hexagonal ice crystals in the atmosphere, J. Geophys. Res., 106, 4845–4870, 2001.